TRANSIENT-KINETIC STUDY OF NI CATALYZED METHANATION: FINAL REPORT

PITTSBURGH UNIV., PA. DEPT. OF CHEMICAL
AND PETROLEUM ENGINEERING
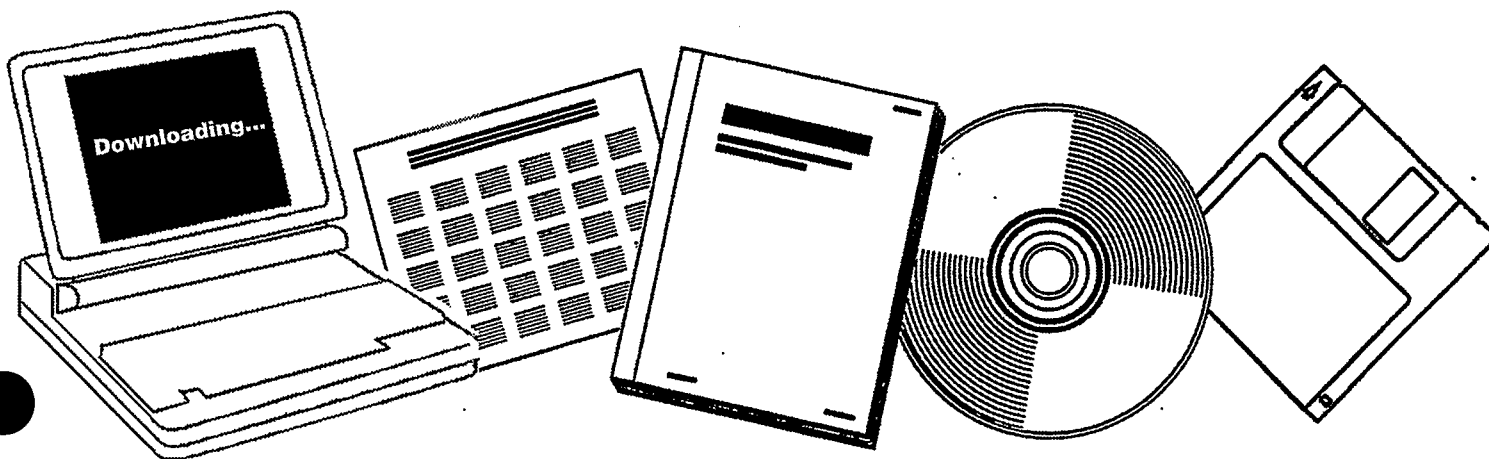
31 AUG 1986

FINAL REPORT

A TRANSIENT-KINETIC STUDY OF Ni CATALYZED METHANATION

by

Paul Biloen and Yee Soong
Department of Chemical and Petroleum Engineering
University of Pittsburgh
Pittsburgh, PA 15261

August 31, 1986

DISCLAIMER

OBJECTIVES AND SCOPE OF WORK

Conversion of synthesis gas (CO/H_2) into fuels and chemicals over transition metal catalysts has been a subject of considerable interest to many researchers over the past 80 years. Naturally, a lot of controversy has arisen regarding the reaction mechanisms, the nature, origin and coverages of reaction intermediates and the catalyst aging process. A key issue is the role of surface carbon either as a provider of reactive intermediates or as a site-blocking catalyst-poisoning agent. Pertinent to this issue is the distribution of the carbidic ad-layer between these two roles, the factors that control the coverages and the extent to which the coverages control the rate of synthesis of methane and higher hydrocarbons.

This study was undertaken to investigate the nature of the rate-determining surface processes in nickel catalyzed methanation utilizing isotopic transient methods. Questions being addressed include:

- What is the mechanism and rate-determining steps for methanation over nickel catalysts?

- Why is the coverage of reaction intermediates low?

- How do the coverages of reaction intermediates and their reactivities vary with reaction conditions and with different catalysts?

- What are the reasons of catalyst aging?

- What is the origin of the H/D isotope effect? What inferences can be drawn from this effect?

- What are the forms and concentrations of adsorbed hydrogen present during methanation over nickel catalysts?

Seeking answers to these questions would, hopefully, provide a better understanding of the methanation reaction in particular and the syngas conversion process in general.

ABSTRACT

The objectives of this study were to investigate the nature and function of the carbidic overlayer, the reaction mechanism operating, the extent of coverage and reactivity of reaction intermediates, as well as coverage of H_2 and CO and the aging processes when methanation occurs over transition-metal catalysts. Isotopic-transient methods were utilized, focusing on three types of nickel catalysts (Raney nickel, 60 wt % Ni/SiO_2 and nickel powder) and employing a differential tubular reactor. A total pressure of 1 bar was maintained throughout except for some experiments on 60 wt % Ni/SiO_2 when pressure was maintained at 1 bar and temperature was varied from 160°C to 250°C. The H_2/CO ratio was varied from 3 to 40.

A mechanism for methanation is proposed which stipulates both adsorbed hydrogen atoms and CO to be in equilibrium with gas phase hydrogen and CO and the dissociation of CO to be a fast and irreversible process. The reaction of surface carbon proceeds through a slow step (carbon-carbon depolymerization or changes in the carbon-metal coordination) and then reacts very rapidly via a reversible sequence of steps to form a CH_x (x = 1-3) group. The CH_{3ad} species further reacts with H_{ad} to form $CH_4(g)$.

The catalyst aging study on Raney nickel showed that the formation of methane occurred via two parallel pathways. The origin of catalyst aging in this particular case is in essence not a process of site blocking, but rather a slow "deterioration" of the Raney nickel itself, causing pronounced kinetic heterogeneity. The coverage of reaction intermediates and their reactivities were found to be significantly dependent on the nature of nickel catalysts.

The origin of an H/D isotope effect was found to be a thermodynamic isotope effect (the coverage of reaction intermediate effect). The overall H/D isotope effect is sensitive to the nature of the nickel catalysts.

The amount of adsorbed CO is not sensitive to the reaction conditions. A large amount of hydrogen coexisting with approximately a monolayer of CO was found under reaction conditions. The adsorbed hydrogen is associated with carbon and with nickel atoms under reaction conditions also.

TABLE OF CONTENTS

Page

TABLE OF CONTENTS

(Continued)

TABLE OF CONTENTS
(Continued)

TABLE OF CONTENTS

(Continued)

LIST OF FIGURES

x

LIST OF FIGURES

(Continued)

LIST OF FIGURES

(Continued)

LIST OF FIGURES

(Continued)

LIST OF FIGURES

(Continued)

LIST OF FIGURES

(Continued)

LIST OF TABLES

LIST OF TABLES

(Continued)

NOMENCLATURE

B   broadening of the diffraction line measured at half-maximum

C_{rea} reactive carbon

C_α reactive carbon

C_{irr} unreactive carbon

C_β unreactive carbon

D   dispersion

D_{eq} degree of equilibrium

d   average metallic particle size of catalysts

E   apparent activation energy

F   fractional isotopic composition

I_{HD} maximum HD intensity during H_2/D_2 exchange

I_{H_2}, I_{D_2} H_2 and D_2 intensity corresponding to the HD intensity at the
           same x coordinates

I^{-*} One type of intermediate

k $(\frac{1}{\tau})$ reactivity of intermediate, or rate constant or constant

k_D reactivity of intermediate in deuterium

k_H reactivity of intermediate in hydrogen

$K_{eq}\ H$ equilibrium constant in hydrogen

$K_{eq}\ D$ equilibrium constant in deuterium

K_{in} equilibrium index

N   the number of surface carbon atoms which act as intermediates,
           or normalization factor

N_s surface exposed atoms

N_{CH_4} turnover number of CH_4 formation expressed as molecules of CH_4 formed per second per metal site

N_{12} the number of surface intermediates I_{12} containing a carbon atom ^{12}C

R   reaction rates

R_H reaction rates in hydrogen

R_D reaction rates in deuterium

r_{CH_4} reaction rate of CH_4

s   metal surface area

TOF   reaction rate per surface-exposed atom

Greek Letters

Θ Bragg angle of diffraction

Θ_{CO} fractional coverage of CO

Θ_H fractional coverage of hydrogen

Θ_C fractional coverage of reaction intermediates

Θ_O fractional coverage of oxygen

τ average lifetime of reaction intermediate (1/k)

λ wavelength of X-ray

ρ density of nickel

1.0 INTRODUCTION

1.1 General Introduction

Methanation,

$$CO + 3H_2 \rightarrow H_2O + CH_4 \qquad (1-1)$$

first reported by Sabatier and Senderens in 1902, has been the subject of a large number of catalytic studies during the past 80 years. It has received much attention during the past few years, primarily because it can convert a low Btu syngas mixture into a high Btu substitute natural gas (SNG). It can also prevent catalyst poisoning by eliminating a small amount of CO present in H_2-rich gases through conversion into CH_4. Because of its intrinsic interest and the close relationship of methanation to other syntheses based on CO hydrogenation, such as the Fischer-Tropsch synthesis of higher molecular weight compounds, the mechanism of methanation is currently an active field of study.

Although methanation is a seemingly simple reaction, its mechanism, intermediates and rate determining step (RDS) are still controversial. In order to gain a better understanding of the mechanism involved, this study addresses a full investigation of mechanism, fractional coverage of reaction intermediates, aging processes, reactivity, rate determining step, H/D isotope effect, and the catalyst coverage by H_2 and CO under reaction conditions. This study, the extensive systematic inquiry into

methanation utilizing isotopic transient methods, provided valuable
fundamental information on the reaction.

1.2 Reaction Mechanisms

The formation of CH_4 from CO and H_2 over Ni catalysts appears to
involve a number of elementary reaction steps including C-O bond
dissociation, H-H bond scission, C-H bond formation, and O-H bond
formation.[1]*

A number of reaction mechanisms, each consisting of various
sequences of these elementary steps, have been proposed to explain
methane formation during methanation.[2-17] Although there are many
excellent review papers[18-24] on methanation, the author does not
intend to report all the findings since the discovery of methanation.
Rather, important results regarding the mechanism of methanation
obtained during the last few years are summarized in Figure 1-1.

In general, the mechanism of methanation can be divided into
several categories:

1. one viewing direct dissociation of CO, not involving the formation
    of CH_nO surface species, as the slow step;[2-4]

2. one involving the formation of CH_nO surface complexes with either
    formation of the CH_nO species or further reaction of the CH_nO
    species as the rate-determining step;[5-7]

---

*Parenthetical references placed superior to the line of text refer
to the bibliography.

A. RDS Involving CO Dissociation

1. $CO* \xrightarrow{RDS} C* \longrightarrow CH_4$ Dalla Betta and Shelef [2]

2. $H_2 \longleftrightarrow 2H*$ $CO \longleftrightarrow CO*$ Ho and Harriott [3]

$CO* + 2H* \xrightarrow[-H_2O]{RDS} C* \xrightarrow{4H*}_{several\ steps} CH_4$

3. $H_2 \longleftrightarrow 2H*$ $CO \longleftrightarrow CO* \xrightarrow{RDS} C* + O*$ $O* + 2H* \longrightarrow H_2O$

$C* \xrightarrow{H*} CH* \xrightarrow{H*} CH_2* \xrightarrow{2H*} CH_4$ Manogue et al. [4]
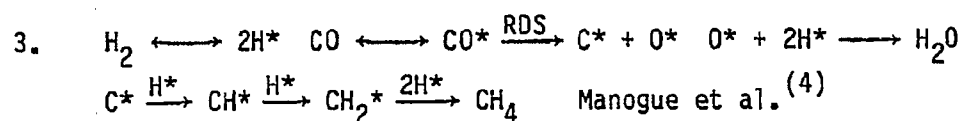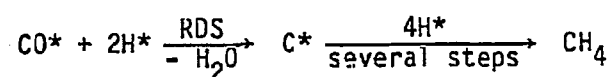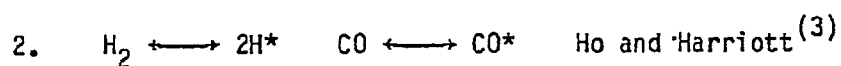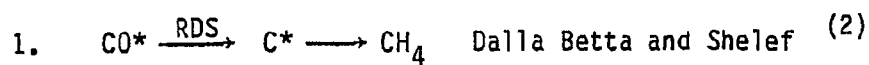
B. RDS Involving CH_nO

1.   General form

$$\underset{M}{\overset{O}{\underset{||}{\overset{||}{C}}}} \xrightarrow{H*} \underset{M}{\overset{H}{\underset{|}{\overset{\diagdown O}{C}}}} \xrightarrow{H*} \underset{M}{\overset{CH_2OH}{\underset{|}{|}}} \xrightarrow[-H_2O]{H*} \underset{M}{\overset{CH_3}{\underset{|}{|}}} \longrightarrow \underset{M}{\overset{CH_4}{\underset{|}{|}}} \longrightarrow CH_4$$

Thompson [5]

2. $CO \longleftrightarrow CO*$ $H_2 \longleftrightarrow H_2*$

$CO* + H_2* \longleftrightarrow CHOH* \xrightarrow[-H_2O]{RDS(+\frac{y}{2}H_2^*)} CH_y* \xrightarrow[fast]{H_2} CH_4$

Vannice [6]

3. $CO \longleftrightarrow CO*$ $H_2 \longleftrightarrow 2H*$

$CO* + nH* \longleftrightarrow COH_n \xrightarrow{RDS} CH_x* + OH_y*$

$CH_x* + (4-x) H* \xrightarrow{fast} CH_4$

$OH_y* + (2-y) H* \xrightarrow{fast} H_2O$ Mori et al [7]
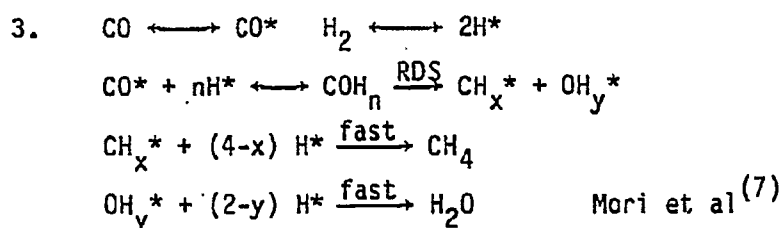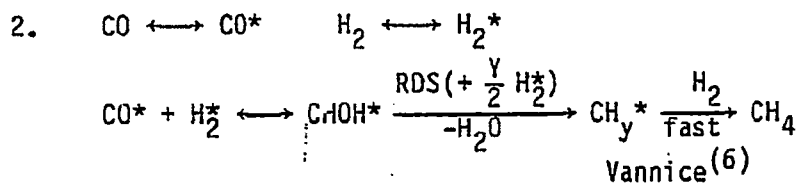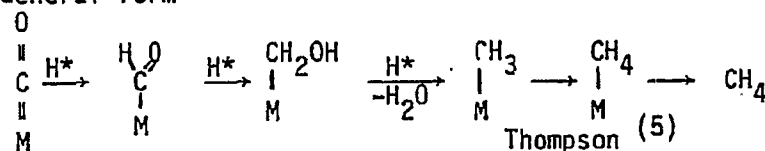
Figure 1-1 Proposed Mechanisms for Methanation

C. RDS Involving CH_x

1. General form

$$CO* \longrightarrow C* + O*$$

$$\underset{M}{\overset{C}{|}} \xrightarrow{H*} \underset{M}{\overset{CH_2}{||}} \longrightarrow \underset{M}{\overset{CH_3}{|}} \longrightarrow \underset{M}{\overset{CH_4}{|}} \longrightarrow CH_4$$

Thompson [5]

2. $CO* \xrightarrow{\text{fast}} CH_x* \xrightarrow{\text{slow}} CH_4$ Biloen and Sachtler[8]

3. $H_2 \longleftrightarrow 2H* \quad CO \longleftrightarrow CO* \longrightarrow C* + O* \quad O* + 2H* \longrightarrow H_2O$

$C* \xrightarrow[+H*]{RDS} CH* \xrightarrow{H*} CH_2* \xrightarrow{2H*} CH_4$ Manogue et al.[4]

4. $CO \longleftrightarrow CO* \longleftrightarrow C* + O* \quad H_2 \longleftrightarrow 2H* \quad O* \xrightarrow{H*} OH* \xrightarrow{H*} H_2O$

$C* \xleftrightarrow{H*} CH* \xrightarrow[+H*]{RDS} CH_2* \xrightarrow[\text{fast}]{2H*} CH_4$ Coenen et al[9]

5. $CO \longleftrightarrow CO* \longrightarrow C* + O* \quad C_* \xleftrightarrow{\text{slow}} C \text{ inactive}$

$H_2 \longleftrightarrow 2H* \quad O* \xleftrightarrow{H*} OH* \xrightarrow{H*} H_2O$

$C* \xrightarrow{H*} CH* \xrightarrow[+H*]{RDS} CH_2* \xrightarrow{H*} CH_3* \xrightarrow{H*} CH_4$ Happel et al[10]

6. $H_2 \longleftrightarrow 2H* \quad CO \longleftrightarrow C* + O* \quad O* \xrightarrow{2H*} H_2O$

$C* \xrightarrow[+2H*]{RDS} CH_2* \xrightarrow{2H*} CH_4$

or $C* \xleftrightarrow{H*} \underset{*}{C} - \underset{*}{H} \xrightarrow[+H*]{RDS} CH_2* \xrightarrow{2H*} CH_4$ Klose and Baerns[11]

7. $M - C \xrightarrow[+H*]{RDS} M \equiv C - H \xrightarrow{H_2} M - CH_3 \xrightarrow{H*} CH_4$ Hayes et al[12]
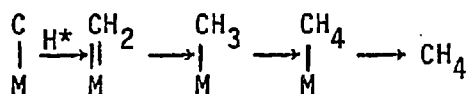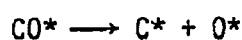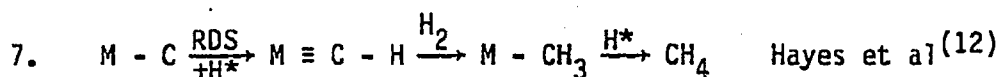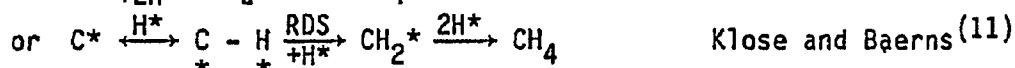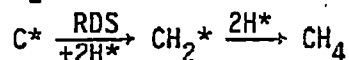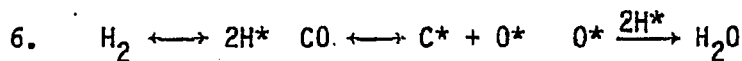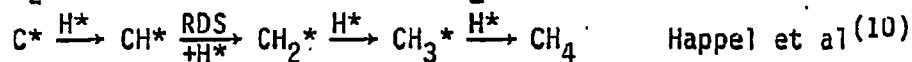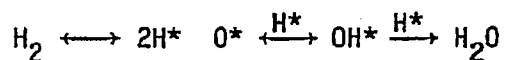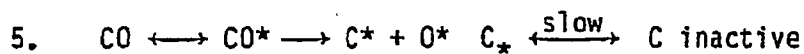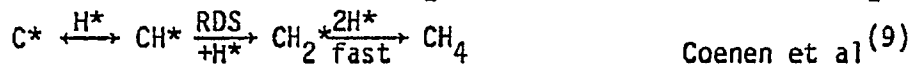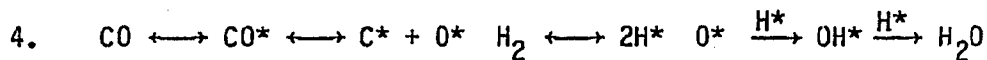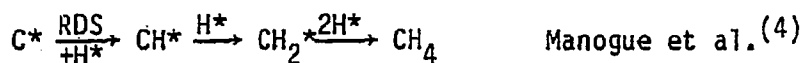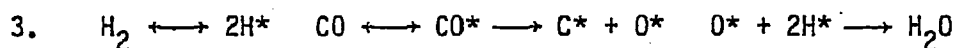
Figure 1-1 Proposed Mechanisms for Methanation (Continued)

D. Balancing between formation and removal of carbon

1. $CO* \longrightarrow C* + O* \quad O* \xrightarrow{2H*} H_2O$

$C* \xrightarrow{4H*} CH_4$ Goodman and Kelley[13]

2. $H_2 \longleftrightarrow 2H* \quad CO \longleftrightarrow CO* \longrightarrow C* + O* \quad O* \xleftarrow{2H*} H_2O$

$C* \xrightarrow{H*} CH* \xrightarrow{H*} CH_2* \xrightarrow{H*} CH_3* \xrightarrow{H*} CH_4$

                                        Bennett and Underwood[14]

3. $H_2 \longleftrightarrow 2H* \quad CO \longleftrightarrow CO* \longleftrightarrow C* + O* \quad O* \xleftarrow{2H*} H_2O$

$C* \xleftarrow{H*} CH* \xleftarrow{H*} CH_2* \xleftarrow{H*} CH_3* \xrightarrow{H*} CH_4$

                                        Bennett amd Stockwell[15]

4. $H_2 \longleftrightarrow 2H* \quad CO \longleftrightarrow CO* \longrightarrow C* + O* \quad O* \xrightarrow{2H*} H_2O$

$C* \xrightarrow{H*} CH* \xrightarrow{3H*} CH_4$ Raupp and Dumesic[16]

E. Others

1. $H_2 \longleftrightarrow 2H* \quad CO \longleftrightarrow CO* \longrightarrow C* + O* \quad O* \xrightarrow{H_2} H_2O$

$M - C + M \xrightarrow{RDS} M_2 - C \xrightarrow{H*} M_3 - CH \xrightarrow{H*} M_4 - CH_2 \xrightarrow{2H*} CH_4$

                                 Hadjigeorghiou and Richardson[17]
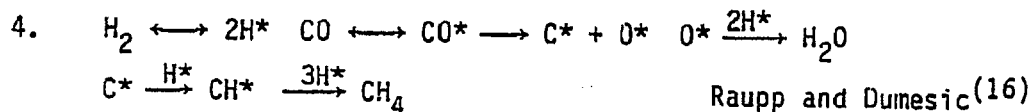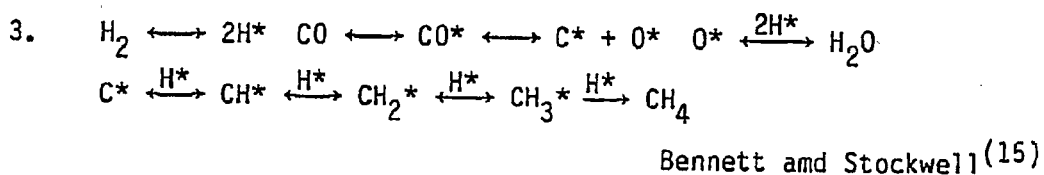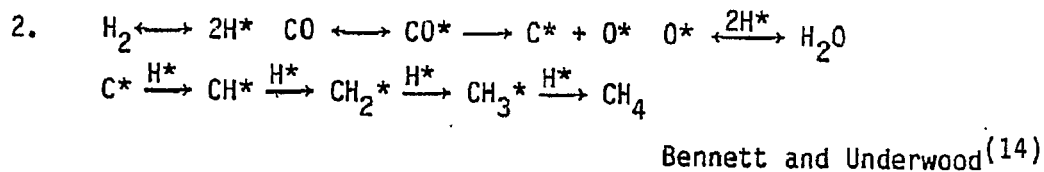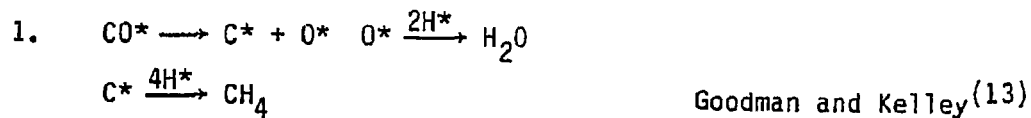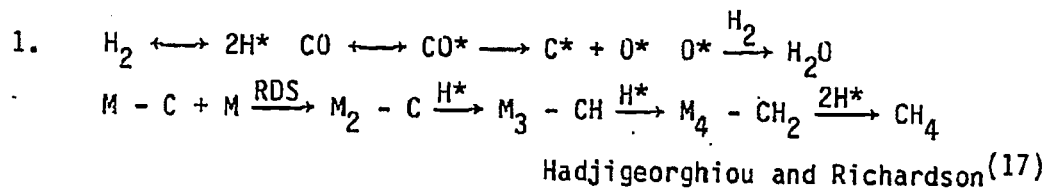
Figure 1-1 Proposed Mechanisms for Methanation (Continued)

3. another regarding carbon, formed by dissociation of CO, followed by reaction between surface carbon and hydrogen atom via CH_x-surface species, with one of the hydrogenation steps as the rate-determining step;[4,5,8-12,25-28]

4. a fourth considering a balance in the carbon formation and carbon removal step during methanation, with neither one a solely rate-determining step;[13-16]

5. the last proposing the change in the carbon-metal coordination to be the rate-determining step.[17]

Despite the numerous studies carried out since the discovery of methanation, no conclusive results concerning the mechanism and rate-determining step of methanation have been obtained and agreed upon. However, with regard to the CH_nO and CH_x surface species and rate-determining step, there is an increasing amount of evidence suggesting the reaction proceeds via an active surface carbon intermediate formed by the dissociation of CO.[18,22] Ponec[23] recently indicated that steady-state methanation on Ni, Co, Rh and Ru, involves an unassisted dissociation of CO. In other words, the sequence is dissociation-hydrogenation.

It is not clear, why different mechanisms exists, even for the same metal. It may be due to the wide variety of experimental conditions used, or due to differences in methodology of obtaining and interpreting kinetic results.

It is found experimentally that the kinetics of methanation is governed by a "power rate";

$$r_{CH_4} = k \, P_{H_2}^x \, P_{CO}^y \qquad\qquad (1-2)$$

where usually x is positive between 0 ~ 1 and y is negative between -1 ~ 0.

Many studies interpret the mechanism of methanation using only steady state kinetic information and an applied Langmuir-Hinshelwood-Hougen-Watson (LHHW) approach. The LHHW procedure includes various assumptions[114] namely (a) an RDS with all other elementary steps in equilibrium, (b) the catalysts surface is energetically homogeneous and (c) no interactions exist between surface adspecies. Based upon those assumptions various equations can be derived which, after certain simplifications, lead to the power rate law. In fact, various mechanisms can be described by the same power rate law.[11,23]

In general, LHHW type models may not correlate well with the observed kinetic data, since the assumptions made are inappropriate under steady state methanation condition. Furthermore, it is insufficient to establish the microscopic mechanism and the RDS of methanation based upon steady state kinetic information with LHHW approach. The study of methanation by the combination of steady state kinetics and isotopic transient methods, on the other hand, may furnish valuable information regarding the reaction pathways.

1.3 Isotopic Transient Methods

In an elementary reaction step of a surface reaction, the reaction rate can be expressed by a simple formula.[25,29-32]

$$TOF = k \; \Theta = \frac{\Theta}{\tau} \qquad\qquad (1\text{-}3)$$

TOF   =   reaction rate per surface-exposed atom (1/s)

Θ =   fractional coverage of reaction intermediates per exposed surface atom

τ =   the average life time of reaction intermediate (s)

$k = \frac{1}{\tau}$ =   reactivity (constant) of intermediate (s^{-1})

Steady-state measurements can only supply the product $k \cdot \Theta$; however, isotopic transient methods can separate k and Θ without disturbing the ongoing surface reaction. Isotopic transient methods have been studied by Happel et al.[10,27,28] and Biloen et al.[25] with the emphasis on isotopic transients in products.

In general, with the reaction maintained at steady state, an isotopic transient can be generated by switching the inlet gas from $^{12}CO/H_2$ into $^{13}CO/H_2$, while keeping the total CO pressure constant (Figure 1-2). Since total CO pressure is constant, and since ^{12}CO and ^{13}CO have identical chemical reactivities, the total CH_4 production remains unaffected. The pool of ^{12}C which furnishes reaction intermediates delays the entrance of ^{13}C into products as $^{13}CH_4$. Biloen
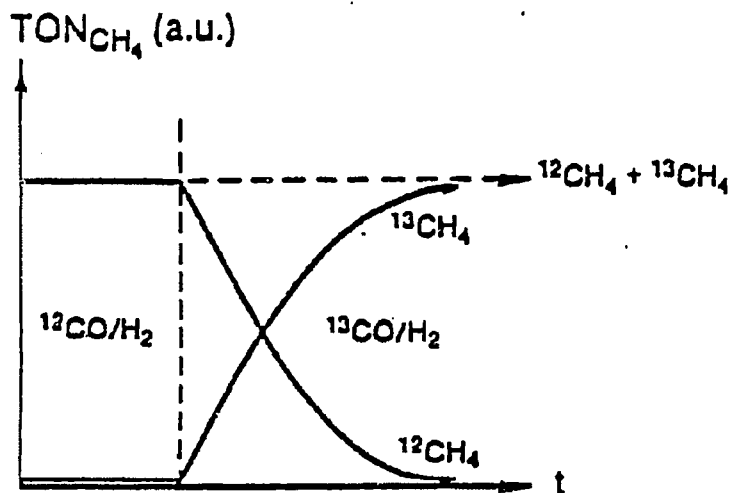
Figure 1-2 Replacing ^{12}CO by ^{13}CO allows for the observation of the full transient-kinetic information without disturbing steady-state catalysis; neither the total CH_4 production nor τ is being affected
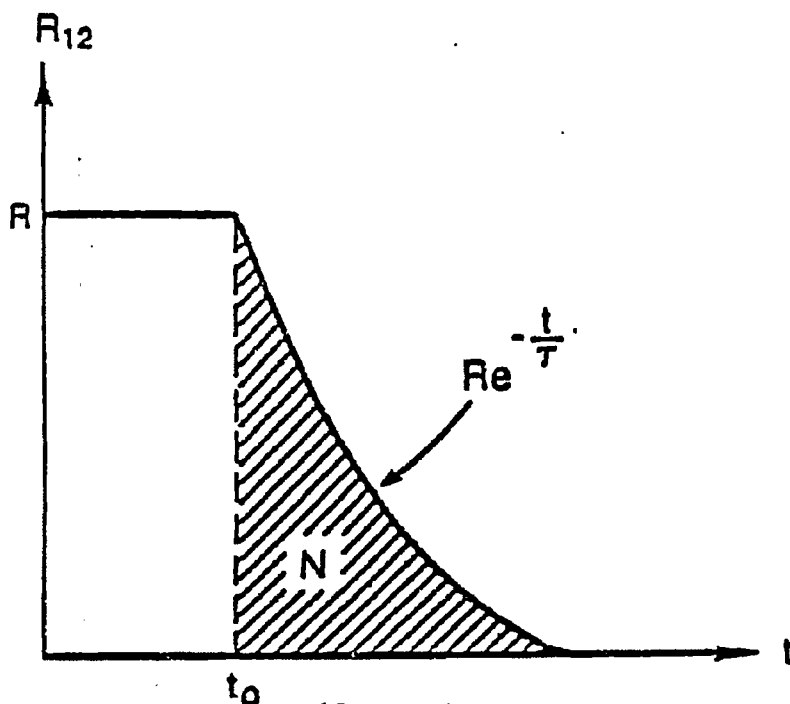
Figure 1-3 Production of $^{12}CH_4$ in $^{13}CO/H_2$ atmosphere derives from ^{12}C-containing surface intermediates. The decay constant reflects the lifetime (τ), the integrated production gives the abundancy (N) of the surface intermediates

et al.[25] and Happel et al.[27,28] suggest this pool may act as one homogeneous reservoir with a delaying action analogous to that of a CSTR. The decay curve of $^{12}CH_4$ is purely an exponential curve (Figure 1-3).

$$F_{12}(t) = \frac{^{12}CH_4}{^{12}CH_4 + ^{13}CH_4} = e^{-t/\tau} \qquad (1-4)$$

The relaxation time constant τ is proportional to the amount of carbon replaced by the new isotope, namely the size of the pool of intermediates (c.f. size of CSTR), and varies inversely to the reaction rate (c.f. the net flows through the CSTR)

$$\tau = \frac{N}{R} \qquad (1-5)$$

$$\tau = \frac{N/Ns}{R/Ns} = \frac{\Theta}{TOF} = \frac{1}{k} \qquad (1-6)$$

where,

N is the number of surface carbon atoms which act as intermediates. Ns is surface exposed atoms, R is rate.

$$\tau = \frac{\Theta}{TOF} \qquad (1-7)$$

$$TOF = \frac{\Theta}{\tau} = k\,\Theta \qquad (1-8)$$

The k and G can be obtained by monitoring the decay response of $^{12}CH_4$ and calculating the area under the decay curve (Figure 1-3). This is the rationale for utilizing step concentration change methods, as done by many authors.[33,34] The rationale for using an isotopic change in reactants is to assure that k is not affected by the removal of one of the reactants.[10,25,27]

1.4 Nature of Surface Carbon

The step involving hydrogenation of atomic "carbidic" carbon from CO dissociation has been proposed as one of the principal elementary steps in methanation over nickel.[18,22,26] The carbidic carbon is heterogeneous in nature, encompassing C_{ads} and CH_{ads}, and perhaps also CH_{2ads}, CH_{3ads}, and polymeric units involving C-C bonds, all having the shared characteristic of not containing oxygen.[8] Previous studies[3,8,22,26,35,36] provide strong evidence for the existence of two carbon forms on the surface of nickel catalysts during methanation: Cα (reactive) and Cβ (less or unreactive). Cα, isolated carbidic or atomic surface carbon atoms bonded to the nickel of high reactivity, is formed by CO dissociation.[18,35] The evidence suggests that C_α reacts with hydrogen on the nickel surface to form methane.[35,37] Cβ, a relatively inactive, polymeric or amorphous carbon, is formed by polymerization or transformation of Cα at relatively high reaction temperatures and/or low H_2/CO ratio.[18,35,37]

In recent studies, Biloen et al.[25] and Happel et al.[10] reported that the active C_{ads} slowly exchanges with large pool of unreactive carbon on Ni/SiO_2. Happel et al.[10] indicate that the unreactive carbon reaches a steady state concentration under reaction conditions, and consequently does not contribute to catalyst deactivation with time.

Bell and Winslow[38] acknowledge a similar observation on Ru catalysts where two forms of carbon, $C\alpha$ and $C\beta$, were observed. $C\alpha$ is more reactive than $C\beta$ and is the principal intermediate in the synthesis of methane. $C\beta$ accumulates rapidly and continuously during the reaction in the first few hundred seconds, but does not strongly inhibit the adsorption of CO or hydrogen. A large amount of hydrogen is associated with $C\beta$ in the form of $C_\beta H_y$, where y is between 1.8 and 2.4.

1.5 Nature of Fractional Coverage of Reaction Intermediates and Their Reactivity

It is interesting to consider why a certain reaction step is fast or slow. Is the rate due to the number of active sites being very high (or low)? Or is it because the reactivity of the active sites is very high (or low)?

The fast or slow step in a reaction pathway can be illustrated as follows. Assume that we have the following reaction steps:

$$R \longrightarrow I_1^* \xrightarrow[k_1]{r_1} I_2^* \xrightarrow[k_2]{r_2} I_3^* \xrightarrow[k_3]{r_3} P \qquad (1-9)$$
$$\quad\ \Theta_1 \qquad\ \Theta_2 \qquad\ \Theta_3$$
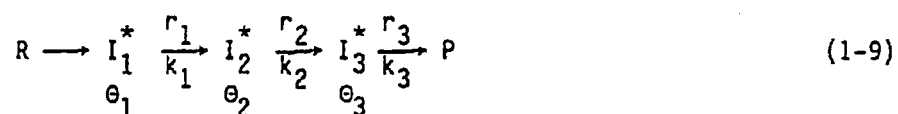
where $r_i = k_i \Theta_i$. The k_i and Θ_i have been defined in Section 1.3. When the reaction is maintained at steady state,

$$r_1 = r_2 = r_3 \qquad \qquad (1\text{-}10)$$

with $k_1 \Theta_1 = k_2 \Theta_2 = k_3 \Theta_3$. Let us confine to r_2 and r_3.

$$r_2 = k_2 \Theta_2 = k_3 \Theta_3 = r_3 \qquad (1\text{-}11)$$

$$\frac{r_2}{k_2} = \Theta_2 \qquad \qquad (1\text{-}12)$$

$$\frac{r_3}{k_3} = \Theta_3 \qquad \qquad (1\text{-}13)$$

Adding (1-12) and (1-13)

$$\frac{r_2}{k_2} + \frac{r_3}{k_3} = \Theta_2 + \Theta_3 \qquad (1\text{-}14)$$

but $r_2 = r_3$, hence we get,

$$r_3 \left(\frac{1}{k_2} + \frac{1}{k_3} \right) = \Theta_2 + \Theta_3 \qquad (1\text{-}15)$$

$$r_3 = \frac{\Theta_2 + \Theta_3}{\frac{1}{k_2} + \frac{1}{k_3}} \qquad (1\text{-}16)$$

for $k_3 \ll k_2$

$$r_3 \approx \frac{\Theta_2 + \Theta_3}{\frac{1}{k_3}} \qquad\qquad (1\text{-}17)$$

If r_3 is limited by k_3, then $I_3^* \to P$ is the slow step.

For $k_2 \gg k_3$, we have $\Theta_2 \ll \Theta_3$ (since $k_2\Theta_2 = k_3\Theta_3$). Thus, in this case, the step having small k and large Θ is defined as the slow step, i.e., $(I_3^* \xrightarrow{slow} P)$. Similarly, the step with large k and small Θ is defined as the fast step $(I_2^* \xrightarrow{fast} I_3^*)$.

Biloen et al.[25] indicate that for methanation and Fischer-Tropsch synthesis over Ru, Co and Ni catalysts, only a small part of the large carbidic overlayer which develops belongs to reaction intermediates. Also, these species are linked to the total carbon reservoir in a reversible fashion.

Similarly, Happel et al.[27,28] report the coverage of reaction intermediates on Ni catalyst is relatively small and varies with the H_2/CO ratio. Data reported by Coenen et al.[9] also shows that in the methanation reaction on a Ni-silica catalyst, only a small fraction of the surface Ni atoms is active (less than 1%).

In experiments with Ni crystals, Goodman et al.[36] determined overlayer coverages from AES. The study shows that large carbidic "overlayers" frequently develop, of which only a part goes to

intermediates. This amount increases with increasing temperature. Bennett and Underwood[14] also report very few reaction intermediates present during methanation over Ni/Al_2O_3.

In a recent study, Happel et al.[10] report that the most abundant reaction intermediate is the CH_{ads} species. Carbidic carbon consists of a relatively small pool of active C_{ads} exchanging with a large pool of carbon, of which neither is active for methanation over Ni catalyst, nor graphitic. Martin and Dalmon[39] also observe that during methanation, only a small part of the Ni surface is covered with the active surface carbon, and the observed rate is most probably directly connected with the concentration of this active species.

Zhang and Biloen[40] reported that the fractional coverage of reaction intermediates for CH_4 on a Co catalyst increases as the H_2/CO ratio is increased.

Recently Bell and Winslow[41] also indicated that the coverage of reactive carbon is low and increases as the temperature is increased.

However, it was concluded in the pulse-technique analysis of the kinetics of the Fischer-Tropsch reaction on Ru by Dautzenberg et al.[42] showed that the low overall activity was not due to a low number of active surface atoms.

From the literature review of this section, it can be concluded that the coverage of reaction intermediates is low, however it is not known yet whether or not this is merely a result of the limited range of reaction conditions utilized so far. Also, it is not known whether these low values derive from intrinsic properties, i.e., catalysis

proceeding only over special atoms such as the ones present at steps or kinks, or whether the majority of the available catalyst surface has been blocked by either unreactive side products or graphitic carbon.

Controversy also exists over the H_2/CO effect on the coverage of reaction intermediates.

The isotopic transient methods provide an excellent way to measure the fractional coverage of reaction intermediates and its reactivity. In order to gain a better understanding of these problems, the study of the fractional coverage of reaction intermediates and reactivity on Ni catalysts as a function of reaction conditions (P, T, H_2/CO) using isotopic transient methods was conducted. The results are discussed in Chapter 4.

1.6 Structure Sensitive

Is methanation over Ni catalysts a structure insensitive (facile) or structure sensitive (demanding) reaction? Numerous studies gave contradictory results.

Goodman and Kelley[13] reporting methanation on Ni(110) and comparing with Vannice's[6] results, concluded that methanation is a structure insensitive reaction. The conclusion was based on the observation of no significant variation both in the absolute value of the reaction rate and in the activation energy as the catalyst changes from small metal particles to bulk single crystals.

Conversely, Dalla Betta et al.[43] suggested that methanation is a structure sensitive reaction. The conclusion is based on the specific steady state methanation activity of Ru, which increases with increasing particle size. Ponec et al.[45] also indicated that methanation is a structure sensitive reaction.

The definition of a structure sensitive reaction or a structure insensitive reaction have been well defined in the literature.[46,47,48] In general, if the reaction rate does not depend on particle size or crystallographic plane, the reaction is said to be structure-insensitive.

A structure-sensitive reaction is defined as having a reaction rate depending on particle size or crystallographic plane. Boudart introduced an operational definition: a reaction is structure sensitive if the rates with the smallest and largest particles differ by a factor of ten or more; for less than ten, the reaction is structure insensitive.[49-51]

The structure sensitivity can be in a sense apparent, caused by the influence of the particle size on side reactions, such as the amount and structure of the carbon deposited on the surface.[52,53]

The effects of changes in the support and metal loading on methanation have been investigated in detail for Ni by Vannice.[6,21] Although large differences were not apparent, specific activity for methanation did vary by factors of up to 5. Dalla Betta et al.[43] also studied the support effect on methanation. The activity per unit surface area of Ni followed the order,

Raney Ni > Ni/Al$_2$O$_3$ > Ni/ZrO$_2$

which also implies that the activity increases as the particle size increases. Idriss et al.[54] suggested that the support effect seems to be originating as a result of:

1. acidity and basicity of the support,

2. the structure of the active sites, the stabilization of intermediates,

3. SMSI (strong metal support interaction) effect.

Recently, Coenen et al.[55] observed that the activity per unit surface area of Ni on silica was strongly dependent on the mean Ni crystallite size (5 - 130 Å). The larger crystallites were particularly active in the reaction, suggesting that on Ni, the methanation of CO requires an ensemble size most abundantly found on larger crystallites.

According to a study of the structure of small particles by Van Hardeveld and Hartog[56], the surface of a particle departs from its characteristic large-particle morphology.

Bartholomew et al.[57] also reported the trend of a higher specific activity at low dispersion i.e., large particle size. Vannice[58] found a lower activity for bulk nickel than for small supported crystallites.

Higher activity (TOF) for larger crystallite sizes of Ni was also reported in many studies.[21,57,59] Taken together, they indicate that the nature of Ni catalyst (support, particle, etc.) does have an effect on methanation rate. However, its effect on to k and Θ is unclear so far.

1.7 Catalyst Aging

In order to improve the stability of any heterogeneous catalyst, it is necessary to assess the dominant aging mechanism(s). It is desirable to develop tools that discriminate between different aging processes such as: reorganizations in the catalyst adlayer (for example, as occurs upon genesis of site-blocking side products) and reorganization of the catalyst itself (for example, as occurs upon annealing, facetting or other forms of surface restructuring). The single-most utilized tool for studying catalyst aging is steady-state kinetics; however, steady-state kinetics lacks the ability to discriminate between different aging mechanisms.

To illustrate why steady-state kinetics has limited incisiveness it is useful to focus on a single unidirectional elementary step corresponding to the unimolecular transformation of A* into B*. For this step, formally denoted by:

$$\ldots \longrightarrow A^* \xrightarrow{\ k_A\ } B^* \longrightarrow \ldots$$
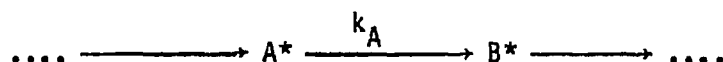
we have

$$TOF_B = \frac{\Theta_A}{\tau_A} = k_A \Theta_A \qquad\qquad (1\text{-}18)$$

in which:

TOF_B: the rate of formation of B* from A*, expressed per surface exposed catalyst atom;

Θ_A: the abundancy of A*, expressed per surface exposed catalyst atom;

τ_A: the lifetime of A* (s);

$k_A = \tau_A^{-1}$:   the reactivity (constant) of A* (s^{-1}).

At best, steady-state measurements can only reveal what happens during aging with the product k.Θ, because TOF (c.f. eq. 1-18) is the only quantity measured. Assessing values for the individual key parameters, k and Θ, is beyond the realm of steady-state kinetics.[60] Accordingly, a site-blocking process primarily affecting Θ becomes indistinguishable from a surface-reconstruction process primarily affecting k.

Reactivities (k) and abundancies (Θ) of surface intermediates do not correspond in a one-to-one manner with model concepts such as the intrinsic activity and abundancy of active sites.[25]. Therefore, we do not want to imply that changes in k and Θ, upon aging, translate necessarily in a one-to-one manner into surface blocking and surface reconstruction. However, k and Θ probably are the most fundamental kinetic parameters which we can measure, even though we have to resort to non-steady-state kinetic methods to measure them.

1.8 H/D Isotope Effect

The details of reaction mechanisms were conventionally studied by investigating the kinetics of reaction under a wide variety of steady state conditions in which the concentrations, temperature, pressure, etc. were in turn made the independent variable. One could then determine (a) the order of the reaction with respect to each reactant and (b) the apparent activation energy. Many possible mechanisms can be inferred from these data. In most cases, unfortunately, this was often largely a matter of guess work, since the proposed mechanism often involved unstable intermediates. The H/D isotopic method allows the details of a proposed reaction mechanism to be checked experimentally.

It is well known that H_2 and D_2 have appreciably different chemical reactivities. It is generally believed that in reactions involving X-H bond rupture, hydrogen and deuterium containing reactants often react at different steady state rates. Utilizing this H/D isotope effect in reaction pathway studies allows one to infer whether or not X-H bond rupture is involved in the rate-determining step.[61-65]

The theory of kinetic isotope effects is usually developed within the "absolute rate theory" or "transition state theory" of Eyring.[66] Assuming an activated or transition state through which the reaction takes place exists, it designates molecules in this state as "activated

complexes". It is further assumed that the molecules passing through the transition state are in thermal equilibrium with the reactant molecules. The rate of reaction is then approximately given by the concentration of activated complex times the average rate of passage of this complex through the activated state to product. By virtue of the second assumption, one may be able to apply the formula of statistical mechanics in calculating the equilibrium concentration of activated complexes. The difficultly arises in the determination of the potential energy of the reacting system as a function of the coordinates of the atoms involved.[65]

In general, the H/D isotope effects can be classified into primary and secondary isotope effects. A primary isotope effect occurs when bonds to the isotopically substituted atom are made or broken in the RDS of the reaction. A secondary isotope effect refers to the effect of an atom which does not take part directly in bond formation or bond breakage in the rate determining step of the reaction on the rate of reaction of isotopic substitution.[61-65]

With respect to the overall reaction rate in H_2 or in D_2, three types of H/D isotope effects are defined: the normal isotope effect ($R_H/R_D > 1$), the inverse isotope effect ($R_H/R_D < 1$) and the absence of isotope effect ($R_H/R_D = 1$).

The literature on the H/D isotope effect on methanation over Ni catalysts is voluminous. Polizzotti and Schwarz[67] indicate a normal H/D isotope effect of 1.86 over a nickel foil. Bennett and Stockwell[15] also report a normal H/D effect of 1.15 over 10%

Ni/Al_2O_3. Coenen et al.[9] show an inverse H/D isotope effect ranging from 0.78 to 1.02, increasing with temperature, decreasing with an increasing P_{H_2}/P_{CO} ratio on a 5% Ni/SiO_2 catalyst. They suggest the addition of adsorbed hydrogen atoms to CH_{ads} as a rate-determining step.

Mori et al.[7] report an inverse H/D isotope effect of 0.77 for methanation on 20% Ni/SiO_2 catalyst at 200°C and the rate-determining step was found to be the dissociation of COH_x species.

Dalla Betta and Shelef[2] found no isotope effect in CO hydrogenation on 5% Ni/ZrO_2 catalyst. Their study also indicates that H unassisted CO dissociation is the rate-determining step.

Bell and Kellner [68] report the inverse H/D isotope effect over alumina- and silica-supported Ru catalysts. According to the study, the magnitude of the isotope effects observed using the silica-supported catalyst is much smaller than that found using the alumina-supported catalyst. This finding implies that the magnitude of the isotope effect may depend on the nature of the support.

Ozaki[61] and Wilson[69] stress that it is not sufficient to justify a rate-determining step based only on an isotope effect. The observed overall H/D isotope effect may result from a combination of the kinetic and equilibrium (thermodynamic) isotope effects.[9,22,23,68]

The H/D isotope effects arise from two sources:[61,69] first, the kinetic and second, the thermodynamic or equilibrium isotope effect. The first of the two sources, the kinetic isotope effect for k_H and k_D is the result of the difference in zero-point energy stored in each X-H, X-D, since the vibrational frequency of a bond with H is always larger

than that with D. Thus it might lead to $k_H > k_D$. Whenever rate-determining X-H bond rupture is preceded by other steps, lumped together in K eq. H.

$$Y-H \xrightleftharpoons{K \text{ eq. } H} X-H \xrightarrow[R_H]{k_H} - - - \qquad (1-19)$$

The overall rate R depends on a kinetic constant, k_H, and a thermodynamic constant, K eq. H.

The other source of H/D isotope effects, the thermodynamic isotope effect, arises from a change in the surface concentration of a reaction intermediate.[70] For the specific case of a heterogeneously catalyzed reaction, the thermodynamic equilibrium constant K eq. H can translate into a coverage in reactive X-H intermediates Θ_{X-H}:

From the same approach

$$Y-D \xrightleftharpoons{K \text{ eq } D} X-D \xrightarrow[R_D]{k_D} - - - \qquad (1-20)$$

It then follows that the magnitude of the overall effect, R_H/R_D, depends on the magnitude of a "kinetic" factor (k_H/k_D) and a "thermodynamic" factor $(K \text{ eq } H/K \text{ eq } D \rightarrow \frac{\Theta_{X-H}}{\Theta_{X-D}})$ [9,23,61] The energy difference between the D-containing and the H-containing products and the reactant largely determine the equilibrium constant ratio, $\Theta_{X-D}/\Theta_{X-H}$. At lower temperatures the value of $\Theta_{X-D}/\Theta_{X-H}$ increases due to an exponential term in the partition function.[70] An inbalance in the vibrational parts of the partition functions of gaseous reactants and adsorbed

species tend to favor $(\Theta_{x-D}/\Theta_{x-H})$ greater than 1. At higher temperatures, the unbalance in the translational parts become dominant, leading to $(\Theta_{x-D}/\Theta_{x-H}) < 1$. The detailed behavior depends critically on factors such as the mobility in the adsorbed state.[61]

For an elementary reaction step,

$$R = k\,\Theta \qquad\qquad (1\text{-}21)$$

H/D substitution affects both k and Θ. It is very difficult to use the steady state kinetics method to determine k (kinetic) and Θ (thermodynamic) effects without applying the statistical mechanics with many assumptions. As indicated by many studies,[9,22,23,68,70] the k (kinetic) and Θ (thermodynamic) effects may compensate with each other. The effect on k has usually been inferred; it conveys whether or not the reaction pathway which leads to the transition state has a component along the X-H bond. Steady state kinetics can only observe the product of k and Θ; however, isotopic transients can separate k and Θ, by measuring both the steady-state and transients in H_2 and D_2 respectively.

$$CO + 3\,H_2 \xrightarrow{\;R_{H_2}\;} CH_4 + H_2O \qquad\qquad (1\text{-}22)$$

$$CO + 3\,D_2 \xrightarrow{\;R_{D_2}\;} CD_4 + D_2O \qquad\qquad (1\text{-}23)$$

This enables one to deconvolute the steady-state isotope effect into a k and a Θ effect.

From the literature review, many questions arise. Is there an isotope effect in methanation? Is it a function of reaction conditions (P, T, H_2/CO)? What is the origin of H/D isotope effect? Is the overall H/D isotope effect a combination of kinetic and thermodynamic effects? Does the magnitude of the H/D isotope effect depend on the nature of the catalyst? Can the H/D isotope effect tell us about the RDS in methanation?

The study of H/D isotopic transients in methanation as a function of temperature, pressure, H_2/CO ratio, and catalysts provided a deeper understanding of the H/D isotope effect.

1.9 H_2 and CO Adsorption

H_2 adsorption is an important elementary step involved in catalytic hydrogenation. It is generally accepted that the adsorption of hydrogen over Ni will follow a Bonhoeffer-Farkas mechanism involving the reactions between adsorbed hydrogen atoms. It has been reported that the adsorption of hydrogen is in dynamic equilibrium, leading to a rate of adsorption equal to that of desorption.[61,71] In general, the amount of H_2 adsorbed will decrease as temperature increases.[61,72]

Much evidence from surface science studies indicates that CO is bonded perpendicularly to the surface of transition metals through the

carbon end of the molecule.[19] The CO molecule can be bonded to one metal atom or bridge over two or more atoms.[73] An increasing dissociation of adsorbed CO occurring as the temperature increases is reported on Ni, Co and Ru.[74] Ponec[23] indicates that C_{ads} and O_{ads} will bind on different sites on the surface. Studies of Ni surfaces[37] show that isolated carbons deposited at temperatures below $300^{\circ}C$ exhibit a fine structure of dispersed carbon comparable to that of metal carbides. This type of carbon has been referred to as carbidic. Decomposition of CO on Ni at higher temperature produces a carbon with an AES spectrum characteristic of graphite forms.[37]

Most CO/H_2 coadsorption studies were done at temperatures far below normal methanation conditions and at UHV conditions with conflicting results. Wedler et al.[75] reported that, in the presence of preadsorbed H_2, much more CO could be adsorbed than on clean nickel films, an indication that adsorbed H induces linear adsorption of CO. It is probably in the presence of hydrogen that the multiple metal bond to CO is not favored.

At $80^{\circ}C$ H_2 is displaced immediately from the Ni film following CO adsorption.[75] Results of the same study show that the nickel surface is capable of simultaneously adsorbing nearly a monolayer of H_2 and CO. Welder et al. defined at least two states of adsorbed H_2: a weakly bound state adsorbing on a region of Ni surface saturated by CO, and a second tightly bound state adsorbing to the Ni atoms through a steady state concentration of vacancies in a nearly saturated CO overlayer. Horgan and King[76] also found that the total moles of H_2 + CO adsorbed

exceeded the coverage of either H_2 or CO alone. Experimental evidence in support of the partially hydrogenated CH_nO surface species was deduced mainly from coadsorption of H_2 and CO where the mutually enhanced adsorption implies surface compound formation.

CO is adsorbed more strongly than H_2; the maximum heat of CO adsorption is about 50% higher than H_2. Therefore, at a low temperature (77^oC) CO displaces H_2 from the surface of Ni almost quantitatively.[18]

While these investigations are consistent in showing an enhancement in adsorption when both H_2 and CO are present in the gas phase, on the other hand, displacement of adsorbed H by CO, blocking of H adsorption by preadsorbed CO, was observed.[18,74,75,76] The discrepancy among the cited findings may be explained by either different experimental conditions (temperature, pressure) or different experimental techniques.

More information on CO_{ad} under reaction conditions over Ni catalysts is available. Most IR studies of the CO hydrogenation on Ni catalyst show that the main surface species is adsorbed CO.[77,78,98]

In their work, Polizzoti and Schwarz[67] indicate almost all of the nickel surface at 230^oC is covered by CO, leaving very few sites for adsorbed hydrogen.

Martin and Dalmon[79] also report that under reaction condition, the surface of the catalyst can be represented as the Ni surface covered by randomly distributed inactive adsorbed CO molecules. Kelley et al.[80] give evidence for a temperature dependent H_2/CO interaction on Raney nickel through Neutron Vibrational Spectroscopy. They indicate that the same adsorbates are found under non-reactive and reaction conditions.

In contrast to what is known about the concentration of adsorbed CO_{ad} on the surface of Ni catalyst, little is yet known about the concentrations of adsorbed H_2.

Happel et al.[10] indicates that for methanation over Ni/SiO_2 under reaction conditions, CO_{ad} seems to occupy almost half of the total sites, hydrogen coverage is substantial and the H_2 adsorbed is in equilibrium with gas-phase H_2. Only a small proportion of the surface is occupied by active carbon.

Bell et al. report H_{ad} and CO_{ad} under reaction conditions over Ru/SiO_2. Under typical conditions, the surface of Ru catalyst will support nearly a monolayer of adsorbed CO. The coverage of this species is relatively insensitive to reaction temperature, or to the partial pressure of H_2 and CO.[81] The chemisorbed H and CO was observed to exchange very rapidly with gas phase H_2, CO. Under reaction conditions, the chemisorbed and gas phase species are in equilibrium[82]. Also, under reaction conditions, the Ru catalyst contains nearly a monolayer of hydrogen together with an equivalent amount of CO. A large amount of hydrogen is found to be associated with β-form of carbon, as $C_\beta H_y$, where y is between 1.8 and 2.4.[38] As the temperature increases, the concentration of adsorbed deuterium decreases substantially.[38] H_2 and D_2 adsorption and dissociation are observed under reaction conditions.[82] The rates of H_2 (D_2) adsorption, reaction and desorption are faster than the rate of hydrocarbon synthesis.

Recently Winslow and Bell[83] reported that there are two forms of hydrogen on unsupported Ni powder at 298 K; a low-energy form which is

in equilibrium with the gas phase and is rapidly displaced from the surface by CO adsorption and a high-energy form which is not in equilibrium with the gas phase and is not displaced by CO adsorption. The low-energy form is ascribed to hydrogen adsorbed on the exterior surfaces of the metal powder. Winslow and Bell[83] propose that the high-energy form may be hydrogen which has migrated along crystal grain boundaries into the interior of the metal powder.

It appears from the literature review that under reaction conditions a large amount of CO and some amount of hydrogen will cover the catalysts, and the CO coverage is not a strong function of reaction conditions (temperature, P_{H_2} and P_{CO}). Much less is known about the forms and concentrations of adsorbed H_2 during methanation over Ni catalysts. The aim of this study was to study the H_2 and CO coverage under reaction conditions over Ni catalysts.

1.10 Objectives and Scope of This Study

A number of mechanisms have been proposed for the synthesis of methane over nickel catalysts.[2-17] Due to differences in methodology of obtaining and interpreting data or due to wide variety of experimental conditions used, the mechanism of methanation still is a subject of controversy. This study utilized isotopic transient methods to investigate the nature of the rate-determining surface processes in

nickel catalyzed methanation. This work was undertaken in order to help provide better understanding to the following questions:

- What is the mechanism and rate-determining steps for methanation over nickel catalysts?

- What are the reasons of catalyst aging?

- Why is the coverage of reaction intermediates low?

- How do the coverages of reaction intermediates and their reactivities vary with reaction conditions and with different catalysts?

- What is the origin of H/D isotope effect? What can be inferred from the H/D isotope effect in methanation?

- What are the forms and concentrations of adsorbed hydrogen present during methanation over nickel catalysts?

The isotopic transient methods have been applied to investigate these problems. Details of these methods are reported in Chapter 2.

Chapter 3 reports the results of an investigation of aging processes in Raney nickel.

The effect of reaction conditions and different nickel catalysts on the coverage of reaction intermediate and its reactivities together with the mechanism of methanation are presented in Chapter 4. Chapter 5 reports the results of a study of H/D isotope effect on methanation.

Results of the forms and concentrations of adsorbed hydrogen present during methanation are presented in Chapter 6.

Overall, this study has sought to establish a better understanding of methanation. The results of this study are summarized in Chapter 7.

2.0 EXPERIMENTAL

2.1 Catalysts and Characterization

Three types of nickel catalysts were used in this study. 60 wt % Ni/SiO_2 (Harshaw 104T, purchased from Harshaw Chemical Co.) with BET surface area 150 m^2/g, pore volume 0.25 cm^3/g was ground and sieved to particles between 0.1 mm and 0.25 mm. After sieving, the catalyst was reduced in flowing H_2 (4 normal liter/hour) at 350°C for 10 hours, then cooled down in H_2 prior to experiment. Raney nickel (Strem, 28-1890, purchased from Strem Chemical Co., manufactured by W. R. Grace Co.), with 8 - 12% wt aluminum, average particle size 50 microns, BET surface area 80 - 100 m^2/g, was diluted with pyrex particles (0.15 mm) at a ratio of 1:2. It was reduced in H_2 (4 normal liter/hour) at 350°C for 12 hours, and then cooled down in H_2 prior to experiment.

Ni powder (purchased from A. D. Mackay Chemicals), with purity 99.999%, particle size -100 mesh was reduced in H_2 (4 normal liter/hour) at 350°C for 4 hours prior to experiment. The average metal particle size for these catalysts was determined by X-ray diffraction using a Cuk_α radiation source and hydrogen temperature programmed desorption (TPD).

The X-ray diffraction method utilized for the determination of the average metal particle size was diffraction line broadening. The estimates of the mean metal particle size were evaluated from the width

of the profiles of the nickel reflection according to the Scherrer equation:

$$d = k\,\lambda/B\cos\Theta \qquad (2\text{-}1)$$

where d is the average particle size in A, λ is the X-ray wave length in A (λ = 1.54178 A for a Cuk_α source), k is a constant (taken as 0.9), B is the observed peak width at half maximum intensity for any reflection, and Θ is the Bragg angle for the diffraction.

Typically, the catalyst was reduced in H_2 at a heating rate of 5°C/min from room temperature to 350°C and held at 350°C for two hours. The reduced catalyst was cooled down in H_2 to room temperature. The H_2 TPD started after flush with Ar at 50 cc/min at room temperature for 0.5 hr, then was operated at a heating rate of 20°C/min from room temperature to 350°C using an Ar flow rate of 50 cc/min. The amount of hydrogen absorbed was calculated based on the area under the TPD curve. The average metal particle size was calculated using the relationship (with the assumption of stoichiometry of H/M = 1) d = 5/sρ, (assuming particles to be cubic with five sides exposed to gas phase) where d is diameter of particle, ρ is the density of nickel, and s is the metal surface area per gram of metal. The results are summarized in Table 2-1. Typical results of XRD are shown in Appendix A.

Table 2-1

Metal Particle Size

Catalyst	XRD d^a(A)	TPD d^b(A)	% (D)^c
60 wt % Ni/SiO$_2$	-	62	13.55
Raney nickel	100	188	4.46
Ni powder	300	900	0.9094

---

a - measured by X-ray diffraction

b - determined by H$_2$(TPD) with the assumption H/M = 1

c - % (D) dispersion calculated by H$_2$ (TPD) result with the assumption

    H/M = 1

2.2 Gases and Apparatus

The gases used for these studies included D_2 (99%), Ar (UHP, 99.9%), Air Products, He (UPS 99.998%), H_2 (UPP, 99.995%), Union Carbide, CO (UHP, 99.8%), CO + 5% Ar (UHP 99.8%) Matheson and, ^{13}CO (99%) Monsanto Research Co.

A differential tubular reactor (6.35 mm OD/4.5 mm ID copper tube with an inventory of approximately 1 cm^3) was used with a high space velocity (larger than 6000 hr^{-1}) to keep conversion low, in order to minimize heat and mass transfer effects. In this way product responses observed during the transient experiments are largely a result of surface kinetic phenomena, not appreciably complicated by the reactor dynamics of the gas phase. The temperatue of the reactor was controlled by a PID controller through four heating elements inside an aluminum bar. Six, Brooks 5850, mass flow controllers were used for controlling the H_2, D_2, ^{12}CO, ^{13}CO, Ar and He flow.

Step changes in concentration were introduced into the reactor by four-way switching valves. Tescom back pressure regulators and pressure transducers were adjusted to ensure that partial pressures are essentially unaffected by the isotope switch.

On-line mass spectrometry was used, by continuous sampling at the reactor outlet. A small part of the outlet stream was routed via a one meter long heated stainless steel capillary (0.1 mm ID) and a Nupro fine metering valve into an Extra Nuclear Model 2750-50 quadrupole mass spectrometer. In order to minimize memory effects, the stainless steel

spectrometer housing was permanently heated ($100^\circ C$). The chamber was pumped with a 90- ℓ/s Leybold-Heraeus turbo molecular pump.

Selection of the mass spectrometer setting and data acquisition was accomplished by using an Apple IIe computer plus a Cyborg Isaac interface. Computer programs for data acquistion and data analysis are presented in Appendix B.

The open electron-impact ionizer was operated at an impact energy of only 22 eV to minimize the interference from OH and O fragments during the $^{12}CO/^{13}CO$ exchange, and from He during the H_2/D_2 exchange. $^{12}CH_4$ is determined at m = 15 and $^{13}CH_4$ at m = 17. $^{12}CD_4$ is determined at m = 18 and $^{13}CD_4$ at m = 21. The fragmentation patterns for CH_4, CD_4, H_2O and D_2O are shown in Appendix A.

In conjunction with MS analysis, gas chromatography was used to analyze the steady-state reactor effluent stream. A Varian 3700 gas chromatograph was used with two packed columns (molecular sieve 5A and Carbosieve S-II) with a thermal conductive detector calibrated with standard gas mixture and with pure CH_4 and pure CD_4 for the study of H/D isotope effect. The experimental set-up is shown in Figure 2-1, schematically.

2.3 CO_{ad} Measurements

When one switches from ^{12}CO (trace Ar) to ^{13}CO at the reactor inlet, there is a time delay between the disappearance of ^{12}CO and Ar at
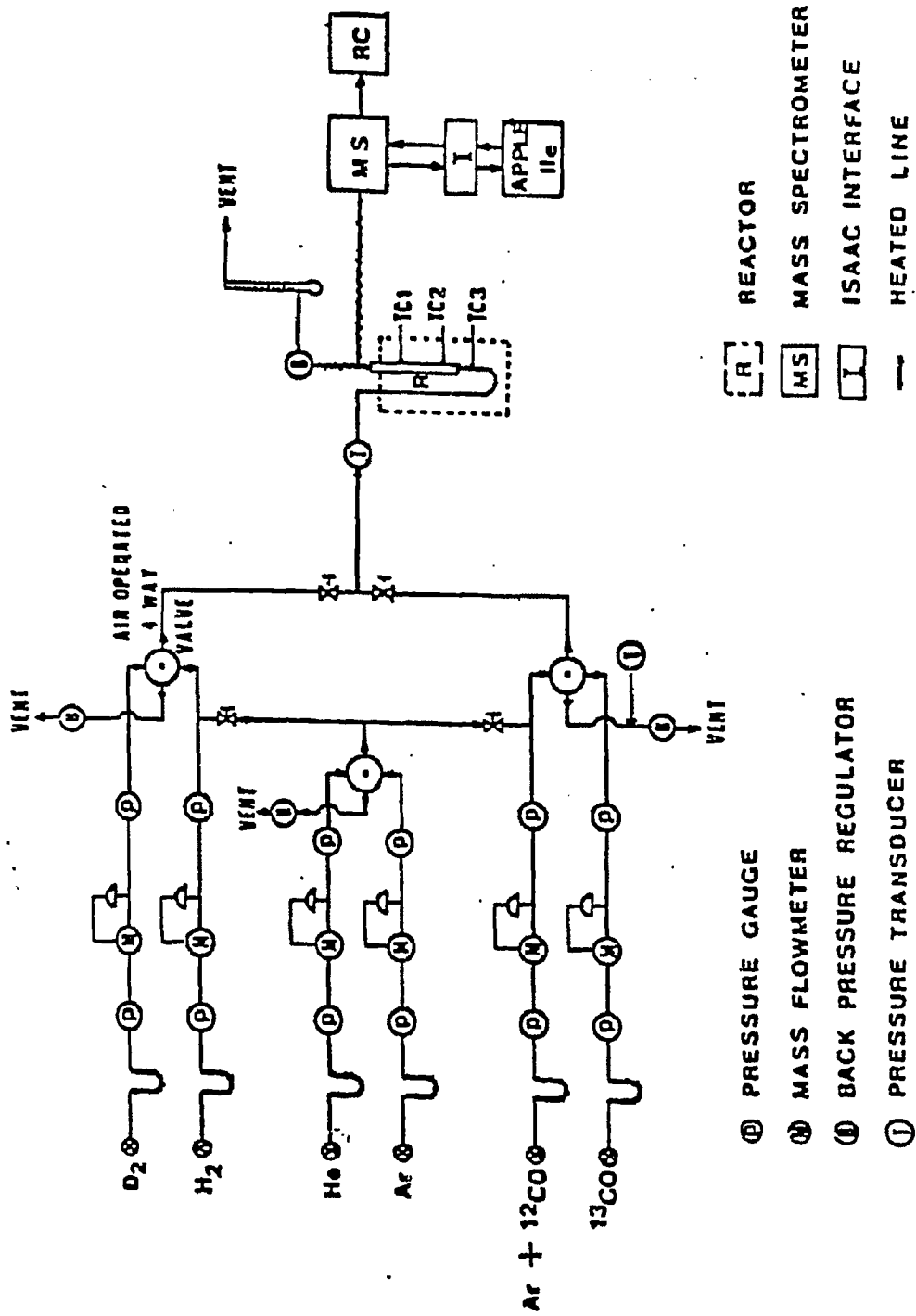
Figure 2-1   Schematic Diagram of Reactor System

- ⓟ PRESSURE GAUGE
- Ⓜ MASS FLOWMETER
- Ⓑ BACK PRESSURE REGULATOR
- Ⓣ PRESSURE TRANSDUCER

- [R] REACTOR
- [MS] MASS SPECTROMETER
- [I] ISAAC INTERFACE
- — HEATED LINE

the reactor outlets. Ar decays first (Figure 2-2). This effect arises from the presence of an inventory of adsorbed ^{12}CO which is not being paralleled by an inventory of adsorbed Ar. This inventory of adsorbed ^{12}CO is being replaced by ^{13}CO and shows up as the area between the Ar and the ^{12}CO decay curve: a chromatographic, frontal elution effect.[25,30,31,32] By multiplying the area between the Ar and ^{12}CO curves (unit:s) by the CO flow rate (units = ml (STP)/s), the amount of adsorbed CO (units: ml step) was obtained.

Similarly, the amount of adsorbed CO can also be determined under reaction conditions (Figure 2-3).

2.4 H_{ad} Measurements

The amount of H_2 adsorbed was measured by D_2 (Ar trace)/H_2 switch, titration method and thermal desorption. A typical result of D_2 (Ar trace)/H_2 exchange is shown in Figure 2-4.

H_2/D_2 Exchange method:

When switching from D_2 (Ar trace) to H_2 at the reactor inlet, there was a time delay between the disappearance of D_2 and Ar, since D(ad) exits from the reactor either as D_2 or HD. The total amount of deuterium as HD (1/2 area under the HD curve) and D_2 (area between Ar and D_2) was used to determine the amount of D_2 absorbed on the catalyst

Figure 2-2 ^{12}CO (Ar) + H_2 $\longrightarrow$ H_2 + ^{13}CO at 110 ^{o}C on 60 wt % Ni/SiO$_2$
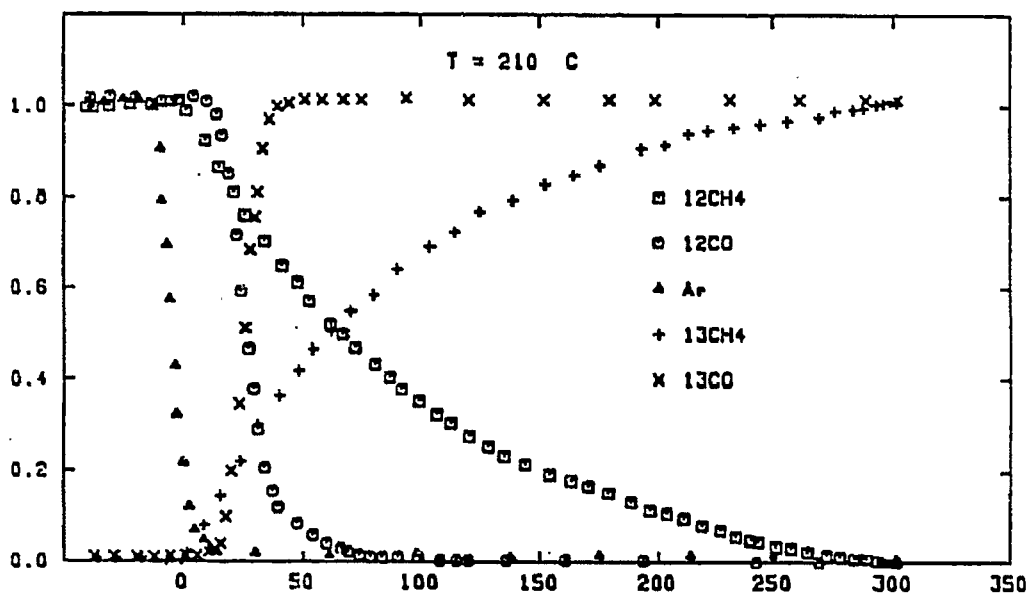
Figure 2-3 ^{12}CO (Ar) + H_2 $\longrightarrow$ H_2 + ^{13}CO at 210 ^{o}C on Raney nickel
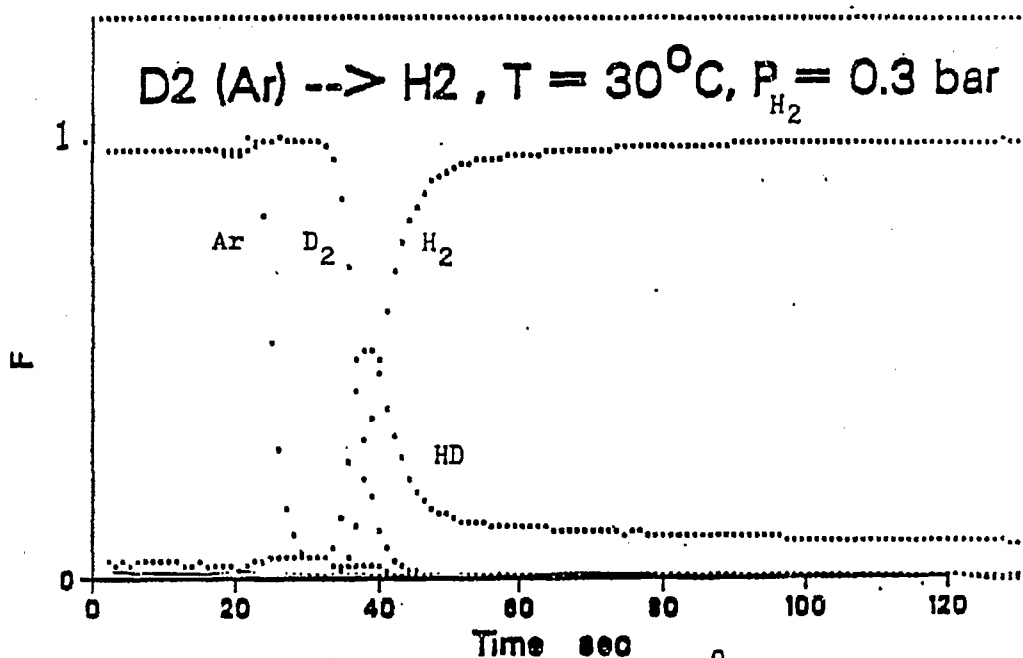
Figure 2-4 D_2 (Ar) $\longrightarrow$ H_2 exchange at 30 ^{o}C, P_{H_2} = 0.3 bar
on 60 wt % Ni/SiO_2
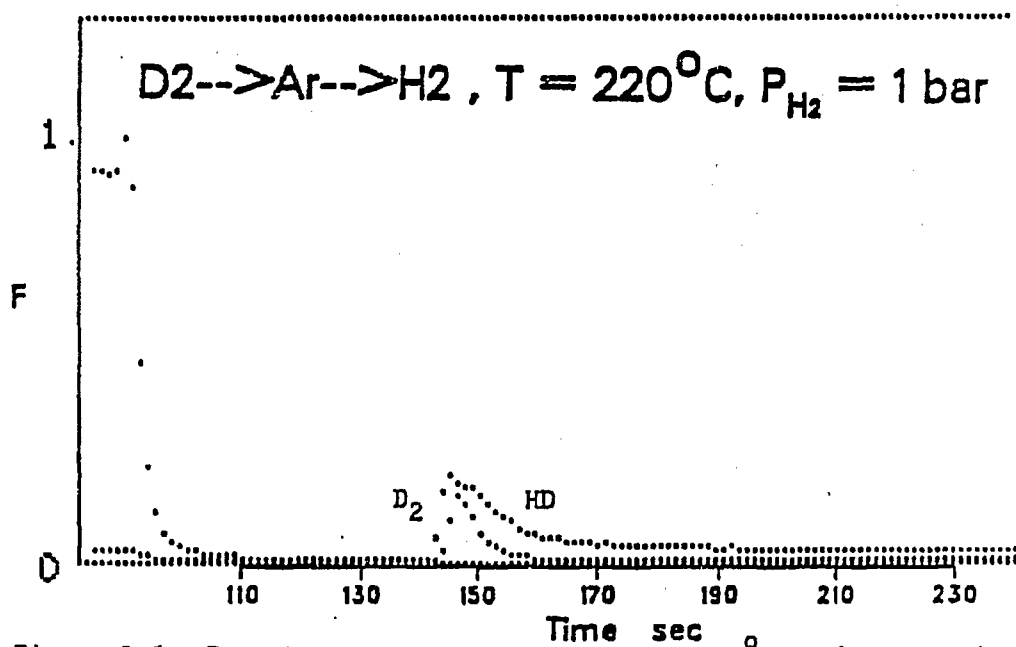
Figure 2-5 $D_2 \longrightarrow Ar \longrightarrow H_2$ titration at 220 ^{o}C on 60 wt% Ni/SiO_2

surface. The amount of H_2 adsorbed can also be determined. Any isotope effect due to substitution of H_2 to D_2 was assumed negligible.[72,84]

Titration method:

First, a reduced catalyst is exposed to flowing D_2, then the catalyst is flushed with Ar for Δ t sec to desorb the weakly and physically adsorbed species. The catalyst is then exposed to flowing H_2 to displace adsorbed D_2 in the form of HD or D_2 (Figure 2-5). The integrated areas from HD and D_2 correspond to the amount of D_2 adsorbed on the catalyst surface. By the same token, the adsorbed H_2 can be measured through $H_2 \to Ar \to D_2$.

Thermal desorption method:

TPD was performed at 1 bar with a heating rate of $10^oC/min$ at varying adsorption temperatures. The gas delivery sequence for TPD is listed as follows: H_2 (T of interest) $\to H_2$ (30 ^oC) $\to$ He (30 ^oC, 30 min) $\to$ He (350 ^oC). The integrated area under the H_2 curve represented the amount of adsorbed H_2 on the catalyst surface. A typical result is shown in Appendix A.

2.5 Reactivity, Fractional Coverage of Reaction
Intermediate and CO_{ad} Measurements

Upon replacement of $^{12}CO_{ad}$ by $^{13}CO_{ad}$ there is a continuous decay of the production of $^{12}CH_4$ (Figure 2-3). This production is fed by ^{12}C containing surface intermediates. Therefore, integration of the area under the $^{12}CH_4$ decay curve yields the total coverage in all those intermediates on the reaction pathway, which are moving forward rather than backward when the surface is replaced by the new isotope. Backward and forward transfer together account for the total amount of intermediates present on the surface. A unidirectional elementary reaction step can serve as a clear-cut boundary between intermediates transferring forward and backward. The chromatographic delay which occurs when substituting $^{13}CO_{ad}$ for $^{12}CO_{ad}$ also delays forward transfer of ^{13}C into $^{13}CH_4$ (c.f. Figure 12 of Ref 25). When total areas under the transient curves are calculated, a correction therefore has to be made on the area measured under the transient $^{12}CH_4$ and $^{13}CH_4$ curve. The correction made is then subtracted from the area under the $^{12}CH_4$ or $^{13}CH_4$ curves (units: s), one half of the area under the ^{12}CO or ^{13}CO curve. This correction is suggested by inspection of Figure 12 of [Ref 25].

One over the area is the reactivity k. TOF = k ⊙. TOF can be obtained from steady-state measurements. ⊙ can also be determined by TOF = k⊙.

These fundamental factors (k,Θ and COad) of methanation were studied systematically by varying reaction conditions over Raney nickel, 60 wt % Ni/SiO_2 and Ni powder. The temperature range varied from $160^{\circ}C$ to $250^{\circ}C$. The H_2/CO ratio varied from 3 to 40. The total pressure was maintained at 1 bar.

For some experiments on 60 wt % Ni/SiO_2, the total pressure was maintained at 4 bar. P_{CO} and P_{H_2} were varied independently by adding the buffering gas, He.

The CO uptake at $110^{\circ}C$ was measured under $H_2/CO > 10$ in order to avoid the formation of nickel carbonyl at low temperatures[57]. The CO_{ad} under reaction condition was determined in-situ from $^{12}CO + H_2 \rightarrow$ $^{13}CO + H_2$ isotopic transient method with the determination of k and Θ respectively.

Under reaction conditions, many reactions may occur simultaneously such as the water gas shift reaction ($CO + H_2O \rightarrow CO_2 + H_2$), Boudouard reaction ($2\ CO \rightarrow C + CO_2$), coke deposition ($H_2 + CO \rightarrow C + H_2O$) and $2\ H_2$ $+ 2\ CO \rightarrow CH_4 + CO_2$. However by choosing $T < 250^{\circ}C$, $P = 1$ bar, $H_2/CO >$ 3, the main product will be H_2O and CH_4.[21,37]

2.6 Catalyst Aging Study

Catalyst aging studies were conducted through two experiments. One was at $T = 238^{\circ}C$, $P_{tot} = 1$ bar, $H_2/CO = 2$ on fresh Raney nickel. A

short exposure to CO at 300°C introduced inactive carbon (successive carbon desposition).

The other experiment studied the aging process at a period of two weeks under $H_2/CO = 2$, $T = 210°C$ and $P_{tot} = 1$ bar condition.

The TOF, k, Θ and CO_{ad} were monitored on both experiments by the isotopic transient method ($^{12}CO + H_2 \rightarrow {}^{13}CO + H_2$).

2.7 H/D Isotope Effect Study

Raney nickel, Ni/SiO_2 and Ni powder were used to study the H/D isotope effect. First the $^{12}CO + H_2 \rightarrow {}^{13}CO + H_2$ isotopic transient method was studied at different reaction conditons. The TOF, k, Θ were obtained. Second, the same catalyst was placed in $^{12}CO + D_2$ and, $^{12}CO + D_2 \rightarrow {}^{13}CO + D_2$ isotopic transient method was studied at same reaction conditions (as in H_2). The TOF, k, Θ were obtained under D_2. The overall H/D isotope effect with the kinetic and thermodynamic effects were compared in H_2 and in D_2.

2.8 H_{ad} Measurement Experiments

The measurement of the amount of adsorbed hydrogen at the catalysts were conducted with Raney nickel, Ni/SiO_2, and to a less extent, Ni powder. The experimental conditions for Ni/SiO_2 included temperatures,

P_{H_2}, Pco (P_{tot} = 4 bar) as independent variables. The experimental conditions fur Raney nickel included temperature, H_2/CO ratio (Ptot = 1 bar) as variables.

3.0 CATALYST AGING STUDY IN RANEY NICKEL

3.1 Background

This chapter reports the behavioral changes of a Raney nickel catalyst during its first 320 hours of exposure to hydrogen-lean syngas, as observed under both steady-state and non-steady-state methods. The activity initially declines at a rate of approximately 0.2% per hour, before "lining out" at approximately 68% of its initial value (Figure 3-1). This behavior is not unlike that observed in other processes, such as catalytic reforming.[85] There is recent literature to help assess what is occurring. Methanation proceeds via carbon-derived surface intermediates, CH_x.[26,27,86,87] With prolonged time on stream these species have the tendency to accumulate,[88] and to deteriorate into a less reactive, hydrogen-poor overlayer.[35,36,88,] For ruthenium and with hydrogenation in hydrogen-only as the criterion, carbon surface species of distinguishable reactivity are already found to be present after a 300-s exposure to CO/H_2.[38] This combined evidence suggests that the following reaction sequence underlies the aging observed in Figure 3-1:

$$CO_{ad} \xrightarrow{k_a} CH_x \xrightarrow{k_b} CH_y \xrightarrow{k_c} C \text{ graph.} \qquad (A)$$

$$CH_x \downarrow k_1 \qquad CH_y \downarrow k_2$$

$$CH_4(g) \qquad CH_4(g)$$
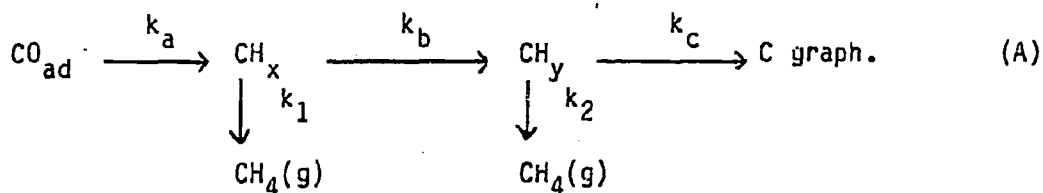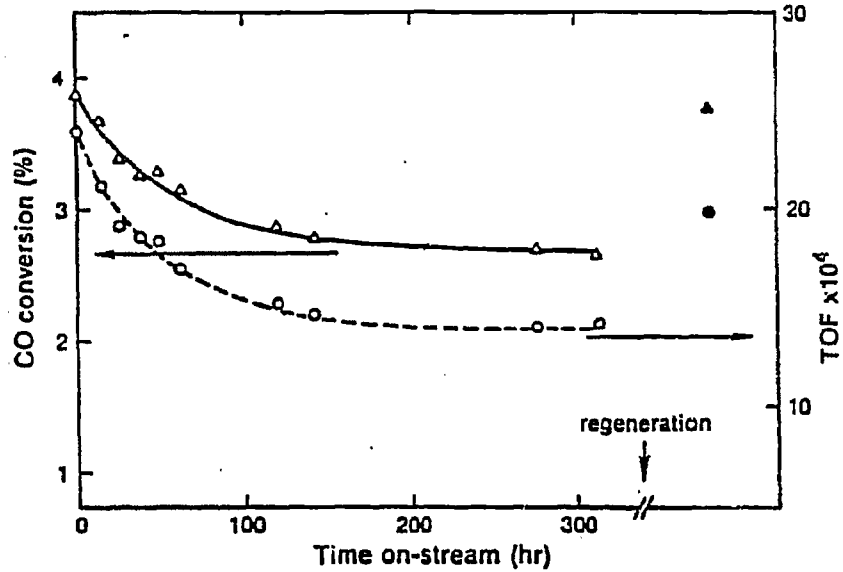
Figure 3-1 Effect of aging on conversion (-) and TOF (---).
Temperature and SV are kept constant during aging. The lining
out time is of the order of 120 h.
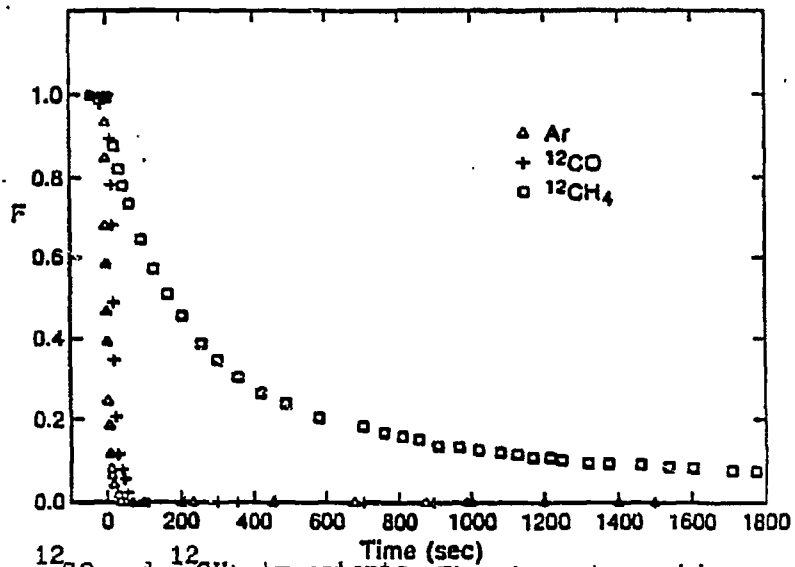
Figure 3-2 ^{12}CO and $^{12}CH_4$ transients. The chromatographic
separation of Ar and CO allows for the calculation of the amount
of CO, adsorbed under steady-state reaction conditions.

According to scheme A the synthesis of methane proceeds mainly via "soft carbon", CH_x. This amorphous, hydrogen-rich[35,36,88] surface species tends to deteriorate slowly (k_b), and leads to a slow buildup of less reactive carbon, CH_y. The 120h line out period is the time needed to balance the CH_y-producing reaction (k_b) by the CH_y-removal reaction (k_2). A very small part of CH_x degrades into "irreactive" carbon, $C_{graphite}$. Very slow building of this terminal species causes the residual decline after the 120 hour lining-out period.

Two features are characteristic of the previous interpretation of Figure 3-1.

(1) Aging is a process that affects the carbon-derived adlayer rather than the nickel-based catalyst.

(2) The rate of lining out coincides with the rate of attaining a steady-state level of CH_y (Scheme A). Therefore, the experimentally observed lining out time of 120 h (Figure 3-1) signals a first-order rate constant, k_2, of the order: $k_2 = 1/120$ h .

During the period represented by Figure 3-1 the feed is repeatedly switched from $^{12}CO/H_2$ to $^{13}CO/H_2$. This leads to a transient-kinetic phenomena: the decay of the $^{12}CH_4$ production, which is being compensated by a concurrent increase in the $^{13}CH_4$ production (Figure 3-5). As the isotopes ^{12}C and ^{13}C have essentially identical chemical reactivity, these experiments provide transient-kinetic information without disrupting the ongoing surface chemistry. From the changes in the transients accompanying the aging we can obtain (k, θ) information.

Although this information does not provide a molecularly detailed picture of the aging process it does lead us to conclude with great certainty that the aging picture discussed in the preceding paragraph and summarized in scheme A is essentially incorrect.

3.2 Experimental

We employed Raney nickel with approximately 8-12 wt % aluminum. After a 12h presintering and reduction period in flowing hydrogen (SV = 6000 1/1/h) we obtained a BET area around 60 m^2/g and surface-exposed nickel area, as measured in-situ with $^{12}CO/^{13}CO$ exchange, around 42 m^2/g. These figures agree with the earlier work of Anderson on low-aluminum Raney nickel.[89] The non-metallic part of the surface probably consists predominantly of Al_2O_3.[89]

Approximately 0.26 ml of (mesh size 60-100) Raney nickel is diluted 1/2 (v/v) with glass beads and loaded into a 1/8" ID copper-tube reactor.

After reduction at 400°C for 12 hours, the catalyst is cooled down in flowing hydrogen to 110°C. CO is introduced, and the surface-exposed metal area is measured via $^{12}CO/^{13}CO$ exchange (see below). The system is then heated in H_2/CO at a rate of 2 deg/min until the reaction temperature (210°C) is reached. All times on stream now quoted are taken relatively to the point in time defined by reaching reaction temperature, 210°C.

3.3 Results

Within 0.5h after coming on stream the catalyst reaches maximum activity. The activity initially declines at a rate of approximately 0.2%/h, but lines out after approximately 120 h on stream. The decline after line out is only approximately 0.7%/24h: Figure 3-1.

When switching off ^{12}CO and Ar simultaneously at the reactor inlet, the production of ^{12}CO at the reactor outlet continues after that of Ar has ceased already (see Figure 3-2 for the effect at 210°C). This frontal-elution, and chromatographic separation of Ar and ^{12}CO is due to the desorption in $^{13}CO/H_2$ atmosphere of an inventory of $^{12}CO_{ad}$, which is not paralleled by desorption of a reservoir of Ar_{ad}.[25,30] This effect is routinely used to determine the number of surface-exposed nickel atoms in-situ. All Θ values and TOF's in this chapter are obtained by assuming a stoichiometry $CO_{ad}/Ni = 1/1$ for the fresh catalyst at 110°C, and at 1 bar atmosphere with $H_2/CO = 10/1$. This assumption is verified by static chemisorption at liquid-nitrogen temperature.[90]

The chromatographic effect is also observable at reaction conditions (Figure 3-2, obtained at T = 210°C, $H_2/CO = 2$), and we calculate a CO coverage close to a monolayer. Moreover, the amount of chemisorbed CO increases rather than decreases with time on stream (Figure 3-3).
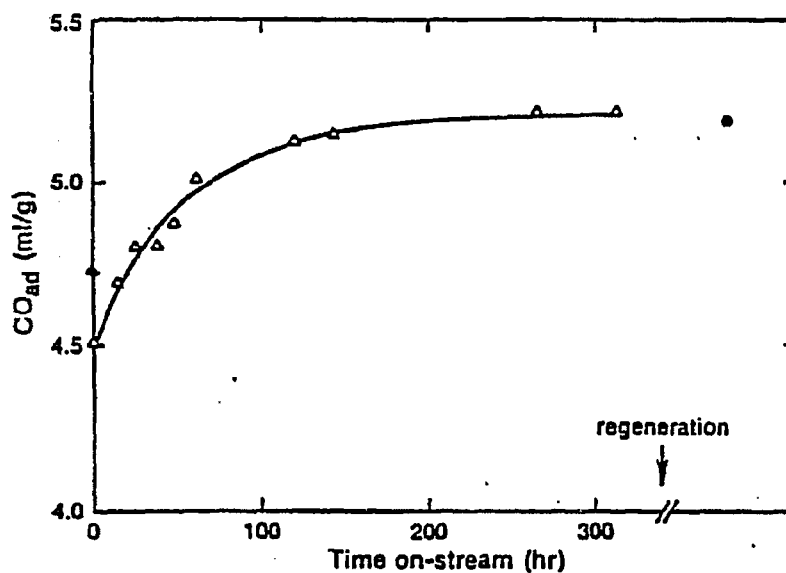
Figure 3-3 The effect of aging on the amount of adsorbed CO.
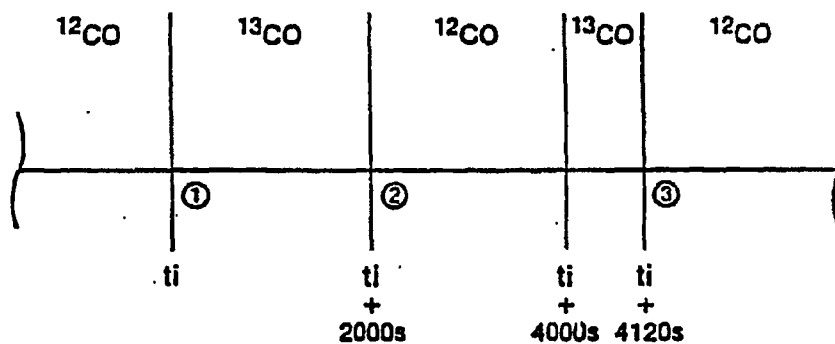
Figure 3-4 For a set of times on stream t_i (t_i = 0.5, 16, 40,
64, and 313 h) we followed a switching pattern which produces
isotopic transients starting at t_i, t_i+ 2000 s, t_i+ 4000 s, and
t_i+ 4120 s.

From the result of Figure 3-3 it may suggest that CO adsorbs on C_{ad}. In order to verify this plausible hypothesis, we conducted a separate experiment. The result of this experiment is shown in Figure 4-17. Figure 4-17 indicates that the successive carbon depositions (short successvie exposure to pure CO at $300^{\circ}C$) lead to a proportional decrease of the TOF and the amount of CO present during steady-state catalysis. It suggests that at reaction conditions, CO does not adsorb on the top of surface blocking C_{ad} and the high value of CO_{ad} are indicative of a largely unblocked surface.

At reaction conditions CO does not chemisorb onto surface carbon. Therefore, we conclude (from Figure 3-3) that during aging the surface-exposed metal area increases rather than decreases, probably due to surface roughening accompanying chemicorrosion.

During aging we regularly switch from $^{12}CO/H_2$ to $^{13}CO/H_2$ and vice versa, in order to observe the isotopic transients. We follow and repeat a particular switching pattern (Figure 3-4), at 15-30h intervals. A set of transients is shown in Figures 3-5, 3-6, and is discussed below.

In response to the switch $^{12}CO/H_2 \rightarrow \,^{13}CO/H_2$ at $t = t_i$, the $^{12}CH_4$ production decreases, and the $^{13}CH_4$ production concurrently increases (Figure 3-5). All ordinate values are relative to their respective steady-state values, $F_{12_{CH_4}} = R_{12_{CH_4}}/(R_{12_{CH_4}} + R_{13_{CH_4}})$, etc. It is evident that the transients obey

$$F_{13_{CH_4}} + F_{12_{CH_4}} = 1 \qquad\qquad (3\text{-}1a)$$
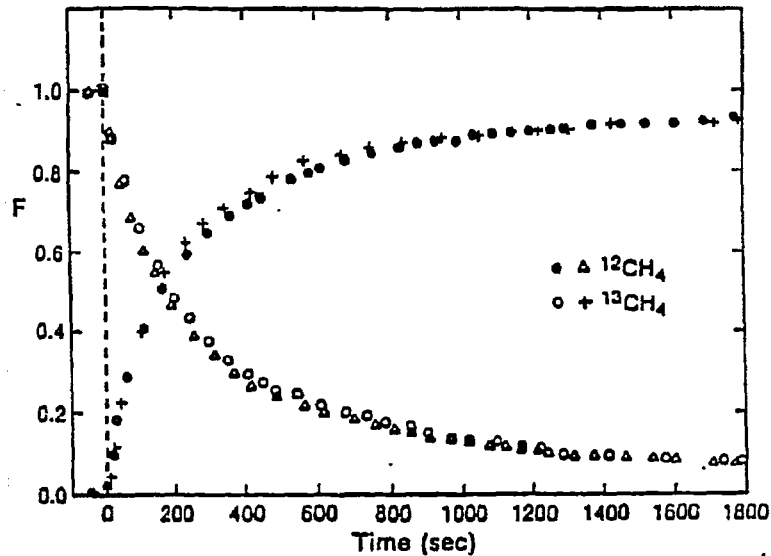
Figure 3-5 Normalized methane transients starting at point (1)
(Fig. 3-4): t_1= 25 h, $(\triangle)^{12}CH_4$,$(+)^{13}CH_4$ and starting at point
(2) (Fig. 3-4): t_1= 25 h + 2000 s, $(\bullet)^{12}CH_4$, $(0)^{13}CH_4$.
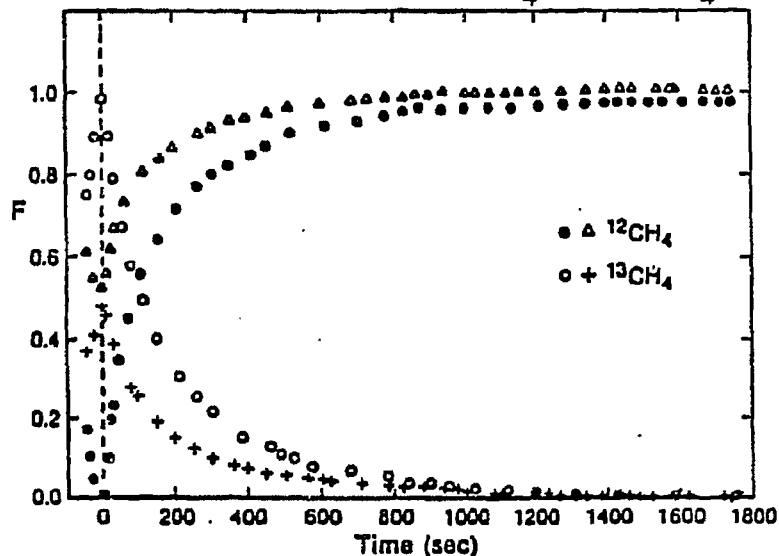
Figure 3-6 Methane transients starting at point (3)(Fig.3-4):
t_1= 25 h + 4120 s, $(+)^{13}CH_4$, $(\triangle)^{12}CH_4$. Because previous
exposure to ^{13}CO encompassed only 120 s the starting value
of $^{12}CH_4$ is above zero, and that of $^{13}CH_4$ below unity.
Normalized transients starting at point (3) (Fig.3-4):$(0)^{13}CH_4$,
$(\bullet)^{12}CH_4$. Compared to the transients measured at (1) and (2)
the tail is lacking ("short exposure changes selectively the
content of short-living reservoirs").

On close examination the transients starting at $t = t_i + 2000s$ (Figure 3-5) are indistinguishable from those starting at $t = t_i$ (with, of course, $^{12}CH_4$ and $^{13}CH_4$ interchanged). . They prove to be indistinguishable also upon curve deconvolution (c.f. Discussion). Figure 3-5 shows four essentially identical transients, provided that we transform the "upcoming" ones (with $\frac{dF}{dt} > 0$) into downcoming ones via the transformation:

$$F^* = 1 - F \qquad (3\text{-}1b)$$

These four transients are averaged, and plotted in Figure 3-7 for each different time on stream, t_i. Figure 3-7 shows one of the main findings of this study, that is, with aging a tail develops in the transients.

The final pair of transients starts at $t = t_i + 4120s$, with $^{13}CH_4$ as the downcoming transient. Prior to switching to $^{12}CO/H_2$, the catalyst being exposed to $^{13}CO/H_2$ for only 120s, $^{13}CH_4$ does start below its steady-state value (Figure 3-6). In order to allow comparison with the other transients we also normalize the third pair of transients (Figure 3-6). This reveals that the normalized $^{13}CH_4$ transient observed after 120s exposure to ^{13}CO differs from that observed after 2000s exposure to ^{13}CO. This is another crucial finding. In Figure 3-8 we plot the (averaged) transients measured at $t = t_i + 4120s$ (t_i = .5h, 16h, 40h, etc.). Unlike the transients measured at $t = t_i$ and $t = t_i + 2000s$, aging does not affect the transients at $t = t_i + 4120s$.
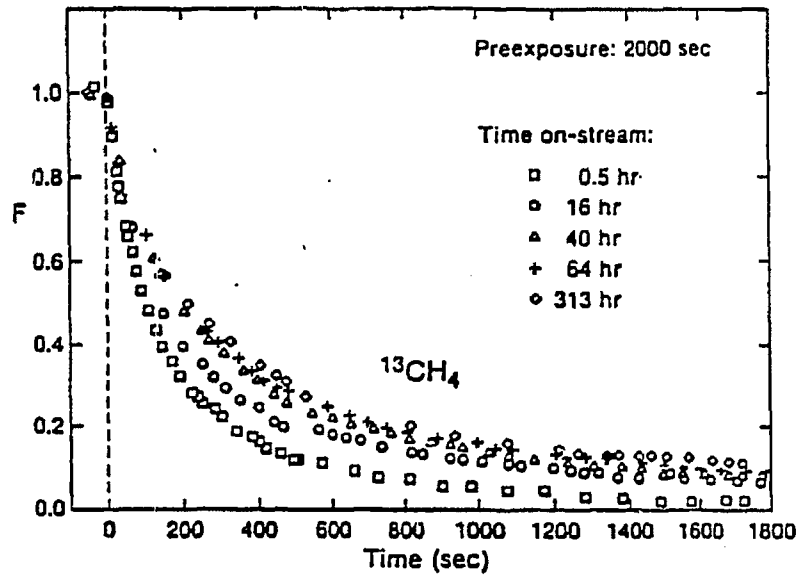
Figure 3-7 As a result of the aging a tail develops in transients measured at t_i and t_i + 2000 s.
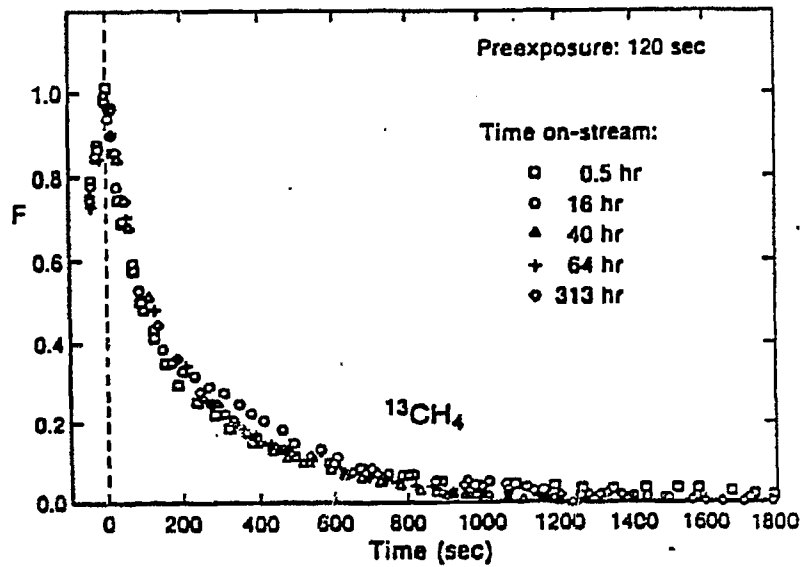
Figure 3-8 The transients measured at t_i = t_i + 4120 s, unlike those measured at t_i and t_i + 2000 s, do not change upon aging.

A few additional experiments will be mentioned in the discussion section.

3.4 Discussion and Conclusion

We start from the observation that the "tails" present in the transients measured at $t = t_i$ and $t = t_i + 2000s$ (c.f. Figure 3-5 and Figure 3-6) are missing in the transients measured at $t = t_i + 4120s$. This puts certain demands on the reaction pathway(s).

Consider first a pathway covering the catalyst with only <u>one</u> type of intermediate, I^{-*}:

$$A(g) \quad \rightarrow \quad I^{-*} \quad \rightarrow \quad B(g) \qquad\qquad (3-2)$$

Assume that A, I^{-*} and B all contain one carbon atom only. Further definitions necessary for a treatment of the isotope transients are

$N_{12}(N_{13})$:   the number of surface intermediates I_{12} (i.e. containing a carbon atom ^{12}C) (moles);

$F_{12} = \dfrac{N_{12}}{N_{12} + N_{13}}$,   with F_{12} (F_{13}) being the fractional isotopic composition of the pool of N surface intermediates, I^{-*};

R: the reaction rate (moles).

A(g) in this treatment is to be identified with CO(g), B(g) with CH_4 and I^{-*} with a carbon-derived surface species. If we assume that prior to t=0 the system is under $^{13}CO/H_2$ for a long time; then:

$$F_{13} = 1; \quad F_{12} = 0 \qquad (3-3)$$

$$N_{13} = N; \quad N_{12} = 0 \qquad (3-4)$$

At t=0 we switch from $^{13}CO/H_2$ to $^{12}CO/H_2$ and for t > 0 we have

$$\frac{dN_{13}}{dt} = -RF_{13} \qquad (3-5)$$

with:

$$dN_{13} = d(N \cdot F_{13}) = NdF_{13} \qquad (3-6)$$

We obtain:

$$\frac{dF_{13}}{dt} = - \frac{1}{(\frac{R}{N})} F_{13} = - \frac{1}{\tau} F_{13} \qquad (3-7)$$

R, N and τ in (Eq. 3-7) all are F_{13}-independent quantities. As ^{12}CO and ^{13}CO have virtually identical chemical properties the change from $^{13}CO/H_2$ to $^{12}CO/H_2$ does not produce any change in reaction rate. Accordingly, (Eq. 3-7) integrates into:

$$F_{13} = (F_{13})_{t=0} \, e^{-\frac{t}{\tau}} = e^{-\frac{t}{\tau}} \qquad (3-8)$$

According to Eq. 3-8 the ^{13}C content of a single homogeneous pool/reservoir of intermediates will, in $^{12}CO/H_2$ atmosphere, decrease exponentially. The rate of decrease will be faster for a smaller pool size (N) and a larger exit stream (R):

$$\tau = \frac{N}{R} \text{ (s)} \qquad (3-9)$$

Therefore, the relaxation constant τ is a characteristic property of the pool/reservoir of intermediates. A single homogeneous pool (CSTR) relaxes with a single relaxation constant, τ.

We now consider transients from partially exchanged systems, such as those starting at point 3 in Figure 3-4. Consider the system to be sufficiently long under $^{12}CO/H_2$ as characterized by $F_{13} = 0$ (t = 0). At t = 0 we switch from $^{12}CO/H_2$ to $^{13}CO/H_2$, and at t = Δt we switch back to $^{12}CO/H_2$ (c.f. to Figure 3-4; t = 0 corresponds to t = t_i + 4000s in Figure 3-4: t = Δt corresponds to t = t_i + 4120s in Figure 3-4). We have

$$F_{13} = 0 \quad (t = 0) \qquad (3-10)$$

$$F_{13} = 1-e^{-\frac{t}{\tau}} \quad (0 < t < \Delta t) \qquad (3-11)$$

$$F_{13} = 1-e^{-\frac{\Delta t}{\tau}} \quad (t = \Delta t) \qquad (3-12)$$

$$\text{and:} \quad F_{13} = (1-e^{-\frac{\Delta t}{\tau}})\, e^{-\frac{(t-\Delta t)}{\tau}} \quad (t > \Delta t) \quad (3\text{-}13)$$

From a comparison of (Eq. 3-13) with (Eq. 3-8) it follows that both, a partially and completely exchanged pool, relax with a single relaxation constant, τ. After normalization the partially and fully exchanged case become indistinguishable. Experimentally, however, the partially exchanged case (Figure 3-6) is distinguishable from the more fully exchanged case (Figure 3-5). This leads us to the conclusion that we are witnessing the combined behavior of at least two pools of surface intermediates.

Figure 3-9A gives one of several possible two-pool models: two pools in series. Below we prove that this configuration cannot be responsible for the difference between transients (1), (2) at the one hand (Figure 3-5) and transient (3) at the other (Figure 3-6). We start with both pools filled with ^{12}C. Upon exposure to $^{13}CO/H_2$ ($t > 0$) we obtain for pool 1 (^1F):

$$^1F_{13} = 1-e^{-\frac{t}{\tau_1}} \quad (3\text{-}14)$$

In a unidirectional pathway the behavior of pool 1 is independent of that of pool 2, and (Eq. 3-14) therefore is identical to (Eq. 3-11). $^1F_{13}$ acts as the input function for the second pool. A mass balance on pool 2 leads to (c.f. Table 3-1):

$$^2F_{13}(t) = 1 - \frac{\tau_1}{\tau_1-\tau_2} e^{-\frac{t}{\tau_1}} + \frac{\tau_2}{\tau_1-\tau_2} e^{-\frac{t}{\tau_2}} \quad (3\text{-}15)$$
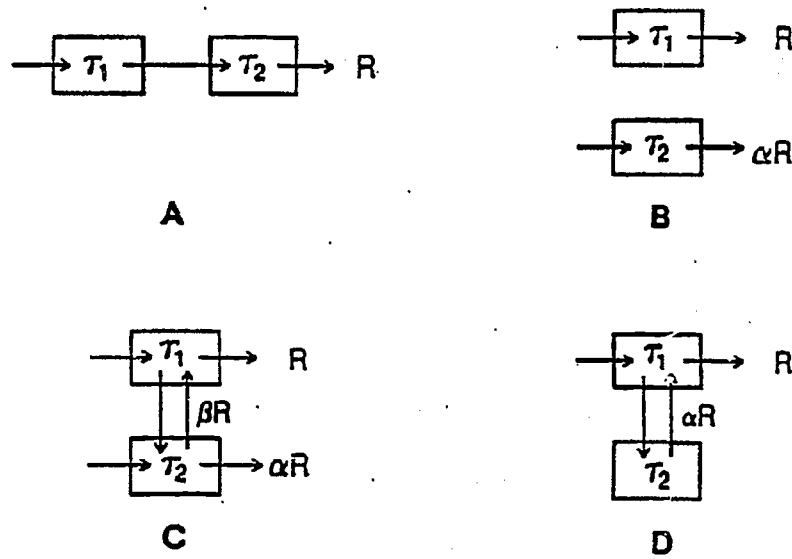
Figure 3-9 Different configurations of two pools of intermediates.
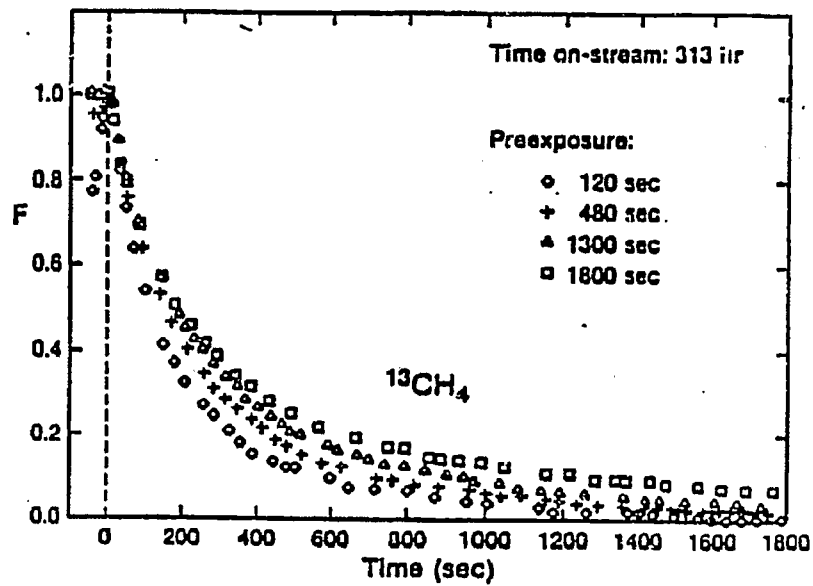
Figure 3-10 The decay of $^{13}CH_4$ varies with the time of preexposure (Δt) to $^{13}CO/H_2$.

TABLE 3-1

Mathematical Models for Aging Study

Model: A (Figure 3-9)

$$F = \frac{\tau_1}{\tau_1 - \tau_2} \exp\left(\frac{-t}{\tau_1}\right) - \frac{\tau_2}{\tau_1 - \tau_2} \exp\left(\frac{-t}{\tau_2}\right)$$

Model: B (Figure 3-9)

$$F = \frac{1}{\alpha+1} \exp\left(\frac{-t}{\tau_1}\right) + \frac{\alpha}{\alpha+1} \exp\left(\frac{-t}{\tau_2}\right)$$

Model: C (Figure 3-9)

$$F = A \exp\left(\frac{-t}{\tau_\alpha}\right) + (1-A) \exp\left(\frac{-t}{\tau_\beta}\right)$$

$$A = \frac{1}{(\alpha+1)} \left(1 + \alpha + \frac{\alpha}{\beta} - \frac{\tau_1 \alpha}{\tau_\alpha \beta}\right) \frac{\left(1 - \frac{\tau_1}{\tau_\beta}\right)}{\tau_1 \left(\frac{1}{\tau_\alpha} - \frac{1}{\tau_\beta}\right)}$$

$$\tau_\alpha, \tau_\beta =$$

$$\frac{}{[\frac{1}{2\tau_2}(1 + \frac{\beta}{\alpha} + \frac{1}{2\tau_1}(1+\beta) \mp \sqrt{(\frac{1}{2\tau_2}(1 + \frac{\beta}{\alpha}))^2 + \frac{(1+\beta)(1 + \beta/\alpha)}{2\tau_1\,\tau_2}}}$$

$$\overline{- \frac{(1+\beta + \beta/\alpha)}{\tau_1\tau_2}]}$$

Model: D (Figure 3-9)

$$F = A \exp\left(\frac{-t}{\tau_\alpha}\right) + (1-A) \exp\left(\frac{-t}{\tau_\beta}\right)$$

$$A = \frac{(1 - \frac{\tau_1}{\tau_\beta})}{\tau_1 (\frac{1}{\tau_\alpha} - \frac{1}{\tau_\beta})}$$

$$\tau_\alpha, \tau_\beta = \frac{1}{[\frac{1}{2\tau_1} + \frac{1}{2\tau_2} + \frac{\alpha}{2\tau_1} \mp \sqrt{(\frac{1}{2}(\frac{1}{\tau_1} + \frac{1}{\tau_2} + \frac{\alpha}{\tau_1}))^2 - \frac{1}{\tau_1\tau_2}}]}$$

Two features are noteworthy, i.e.,

$$^1F_{13}(t) > {}^2F_{13}(t) \tag{3-16}$$

and

$$\left(\frac{d\ ^2F_{13}}{dt}\right)_{t=0} = 0 \tag{3-17}$$

The features (Eq. 3-16) and (Eq. 3-17) arise essentially from the same effect: pool 1 delays the entrance of ^{13}C into pool 2.

If we leave the system for a time Δt in contact with $^{13}CO/H_2$, and then switch back to $^{12}CO/H_2$, the partially exchanged pools will relax as ($t > \Delta t$):

$$^1F_{13} = (1-e^{-\frac{\Delta t}{\tau_1}})\ e^{-(\frac{t-\Delta t}{\tau_1})} \tag{3-18a}$$

and

$$^2F_{13} = \frac{\tau_1}{\tau_1-\tau_2}\ e^{-(\frac{t - \Delta t}{\tau_1})} -$$

$$\frac{[(\tau_2 e^{-\frac{\Delta t}{\tau_2}} + \tau_1 (1-e^{-(\frac{-\Delta t}{\tau_1})})]\ e^{-(\frac{t-\Delta t}{\tau_2})}}{\tau_1 - \tau_2} \tag{3-18b}$$

It emerges that:

$$\left(\frac{d^2F_{13}}{dt}\right)_{t=\Delta t} > 0 \qquad\qquad (3\text{-}19)$$

i.e., in $^{12}CO/H_2$ atmosphere the ^{13}C content of pool 2 initially increases before it decreases. In essence, this is the consequence of the fact that ^{13}C ex-^{13}CO penetrates into pool 1 <u>before</u> it penetrates into pool 2. This leads to equation (Eq. 3-16), and therefore to (Eq. 3-19).

In the actual experiments we observe (c.f. Figure 3-6)

$$\left(\frac{d^2F_{13}}{dt}\right)_{t=t_i+4120s} < 0 \qquad\qquad (3\text{-}20)$$

This leads us to reject the proposition that the difference between the partially and more fully relaxed transients derive from the effect of two or more pools <u>in series.</u> We conclude that the observed effects derived from two or more pools <u>in parallel.</u>

For two independent reservoirs (Figure 3-9B) the combined relaxation is merely the sum of that of the two constituents:

$$^{13}F_t = \frac{1}{1+\alpha} e^{-\frac{t}{\tau_1}} + \frac{\alpha}{1+\alpha} e^{-\frac{t}{\tau_2}} \qquad\qquad (3\text{-}21)$$

in which F_t is the isotopic composition of the completely mixed exit streams of the two pools. For $\tau_2 \gg \tau_1$ an exponential decay with a "tail" originates (Eq. 3-21), similar to the responses observed at $t=t_i$ and $t=t_i+2000s$ (Figure 3-7).

In order to find the behavior of a partially exchanged system of two parallel reservoirs we start with both systems containing ^{12}C exclusively (t=0). After exposure to $^{13}CO/H_2$ for a period Δt we have:

$$^{13}F_1 = 1-e^{-\frac{\Delta t}{\tau_1}} \tag{3-22}$$

and

$$^{13}F_2 = 1-e^{-\frac{\Delta t}{\tau_2}} \tag{3-23}$$

Switching back to $^{12}CO/H_2$ at $t > \Delta t$ leads to

$$^{13}F_t = N\ [(1-e^{-\frac{\Delta t}{\tau_1}})\ \frac{1}{1+\alpha}\ e^{-\frac{t-\Delta t}{\tau_1}} + (1-e^{-\frac{\Delta t}{\tau_2}})\ \frac{\alpha}{1+\alpha}\ e^{-\frac{t-\Delta t}{\tau_2}}\ ] \tag{3-24}$$

with N as normalization factor.

It follows that an exposure $\Delta t \ll \tau_2$ leads to a suppression of the component $e^{-\frac{t-\Delta t}{\tau_2}}$ in the subsequent relaxation. For a sequence $^{12}CO/H_2$ → $^{13}CO/H_2(\Delta t)$ → $^{12}CO/H_2$ the slowly relaxing reservoir does not fill appreciably with ^{13}C in the period Δt. Therefore it does not produce a pronounced amount of ^{13}C in the subsequent $^{12}CO/H_2$ stage: the "tail" being absent. This is what we observed experimentally (Figure 3-8).

In order to verify the above we measured on stream, after two weeks a series of transients in $^{12}CO/H_2$, obtained after exposing the catalyst to $^{13}CO/H_2$ for a period Δt which varied between 120 s and 1800 s. From

the responses (Figure 3-10), it emerges that the $\tau \approx 1000$ s component (the "tail") in the relaxation pattern increases with increasing exposure, Δt. This result confirms that we are working with reservoirs positioned in parallel rather than in series.

The other "two-reservoirs-in-parallel" models (Figure 3-9C,D) give analytical solutions:

$$F = A e^{-\frac{t}{\tau_\alpha}} + (1-A) e^{-\frac{t}{\tau_\beta}} \qquad (3\text{-}25)$$

which are indistinguishable from the solution given in (Eq. 3-15) for model 3-9B (c.f. Table 3-1). As the time (t) and frequency ($\frac{1}{\Delta t}$) responses are related in a one-to-one manner, these models also cannot be distinguished by looking for variation 'n relaxation with varying exposure, i.e., by experiments of the type depicted in Figure 3-10. However, all what models 3-9B-D share is that at least for part of the pathway from CO to CH_4, there are two parallel, independent routes. We will focus on this feature, and what it means in terms of processes underlying aging. In doing so we confine ourselves to model 3-9B with its simple relations (c.f. Eq. 3-25 with Eq. 3-15 and Figure 3-9B):

$$\tau_\alpha = \tau_1 \qquad (3\text{-}26a)$$

$$\tau_\beta = \tau_2 \qquad (3\text{-}26b)$$

$$A = \frac{1}{1+\alpha} \qquad (3\text{-}26c)$$

Our conclusion, however, will also be valid whenever Figure 3-9C,D rather than Figure 3-9B describes the actual system.

The preceding analysis of the relaxation of partially exchanged systems indicates the following.

(1) We are dealing with at least two pools of intermediates.

(2) These pools are positioned (partially) in parallel rather than in a series.

(3) Such a parallel configuration leads to a relaxation curve consisting of a sum of two exponentials.

(4) The relative contribution of the component with the shorter time constant can be accentuated by measuring the relaxation short exchange times.

It follows that we should determine τ_1 (with, by definition, $\tau_1 < \tau_2$) from the transients starting at $t = t_i + 4120s$ (c.f. Figure 3-4). These transients are given in Figure 3-8. From inspection of Figure 3-8 it emerges, and this is one of the main findings in the present study, that τ_1 is highly independent of catalyst aging.

An unweighed least-square fit of Figure 3-8 to

$$F(t) = (A-B) \; e^{-\frac{t}{\tau_1}} + B \qquad (3-27)$$

yields

$$\tau_1 = 120 \pm 20s$$

and

$$B = 0.05 \pm 0.01$$

with the values quoted as $\pm$ being single standard deviations. Component B has been included to account for both unresolved low-frequency components and uncertainty in separation of the signal from the background.

With the value $\tau_1 = 120s$ obtained from the transients measured at $t = t_i + 4120s$ we deconvoluted the transients measured at $t = t_i$ and $t = t_i + 2000s$ into

$$F(t) = (A-B)\ e^{-\frac{t}{120}} + (1-A-B)\ e^{-\frac{t}{\tau_2}} + B \qquad (3-28)$$

No trend of τ_2 with time on stream is discernible, and we obtain

$$\tau_2 = 850 \pm 200s$$

What is changing with time-on-stream, however, are the relative contributions to the total methane production of the 120s and 850s reservoir. Figure 3-11 gives the amplitudes of the 120s and 850s components (Eq. 3-28) as a function of time on stream. The 850s component (the "tail") increases at the expense of the 120s component, and lining-out takes place parallel with that of the activity (compare
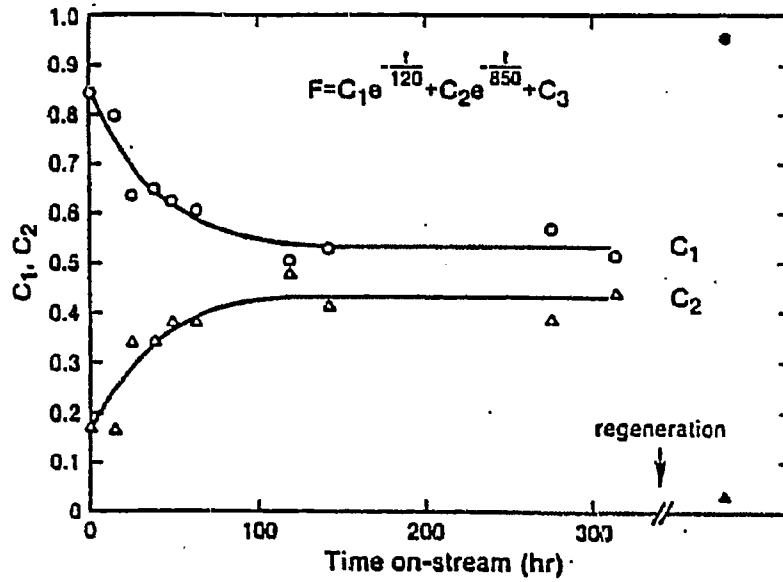
Figure 3-11 Variation with line out of the relative contribution of the $\tau_1 = 120$ s and $\tau_2 = 850$ s component to the CH_4 make.

$$F = C_1 e^{-\frac{t}{120}} + C_2 e^{-\frac{t}{850}} + C_3$$
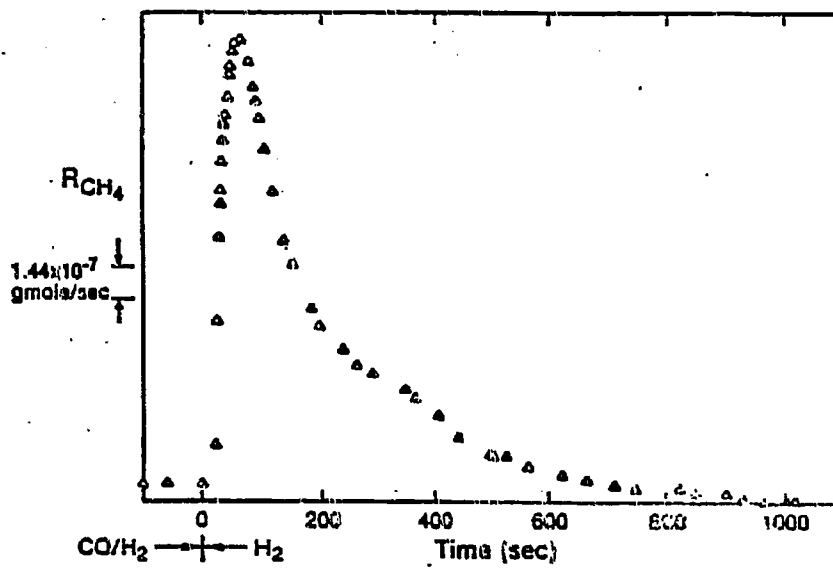
Figure 3-12 Methane production in pure H_2 signals a large reservoir of (dissolved) carbon.

Figure 3-11 with Figure 3-1). It is apparent that the initial decrease in TOF and the development of a reservoir of intermediates with reactivity $k \approx 1/850s$ are manifestations of the same lining out phenomenon.[1]

In the background, we considered, as a possible cause of the lining out phenomenon, the building up of less reactive carbon, CH_y, balanced after approximately 120h by the removal reaction (k_2)

$$CO(g) \xrightarrow{k_a} CH_x\text{-soft} \xrightarrow{k_b} CH_y\text{-hard} \xrightarrow{k_c} C_{graphite} \qquad (A)$$
$$\downarrow k_1 \qquad\qquad \downarrow k_2$$
$$CH_4(g) \qquad\quad CH_4(g)$$

Because of what has been inferred about reservoirs in series versus reservoirs in parallel (Figure 3-9) we have to consider alternatives such as

$$CO(g) \overset{k_a}{\underset{k_b}{\lessgtr}} \begin{array}{l} CH_x\text{-soft} \xrightarrow{k_1} CH_4(g) \\ (\updownarrow) \\ CH_y\text{- hard} \xrightarrow{k_2} CH_4(g) \end{array} \qquad (B)$$

or

$$CO(g) \xrightarrow{k_a} CH_x\text{-soft} \xrightarrow{k_1} CH_4(g) \qquad (C)$$
$$k_2 \updownarrow k_{-2}$$
$$CH_y\text{-hard}$$

---

[1]We mention that deconvolution of the tailing transients with **both** τ_1 and τ_2 as fitting parameters leads to considerably more noise than the procedure followed at present, i.e., changing the pre-exposure time and inferring τ_1 from the transients of the partially exchanged system.

These and similar schemes share that CH_y-hard gradually builds up, and that lining out is caused by a CH_y-removal reaction balancing the CH_y-formation reaction. Lining out occurs at an interval of the order of 120h (Figure 3-1). This implies that the formation/removal reaction equilibrates in about 120h, <u>and further that CH_y-hard itself has a lifetime τ of about 120h.</u> However, the transient experiments demonstrate CH_y-hard to have a lifetime of the order of 850s. This rules out all schemes such as A-C, that features build-up of CH_y-hard as the cause of the lining out.

Now we consider surface blocking by a third type of carbon, say $C_{graphite}$, exhibiting a $\tau = 120h$. The contribution of such carbon to the transients will vanish in the background. Actually, there is ample evidence for a large pool of additional carbon (see below). However, this pool apparently does not block the surface. We infer this from the following observations:

- The total CO_{ad}· uptake increases with time on stream (Figure 3-3).

- The combined coverage $\theta_{CH_x} + \theta_{CH_y}$ increases with time on stream, excluding surface blocking to underlie the lining out.

Above, we eliminated a change in the reactive and a change in the irreactive (i.e., merely surface blocking) overlayer as primary causes of the line out phenomenon. <u>Therefore, we conclude that rather than a change in the adlayer, the line out reflects a slow change in the catalytic properties of the "nickel" itself.</u>

We reached the previous conclusion without making mechanistic assumptions or drawing on any evidence but that provided by the transients. However, we cannot proceed much beyond this point. We subjected the aged catalyst at reaction temperature to an exposure of pure hydrogen. The following findings are evident

(1) A carbon reservoir of over ten monolayer equivalents appears (Figure 3-12);

(2) The size of the reservoir (i.e., N), together with the rate of removal R in CO/H_2 atmosphere (an upper limit can be calculated from the background in the transients) signals carbon with a long life time:

$$\tau = \frac{N}{R} > 10h$$

(3) The carbon removal restores the original shape of the transients (Figure 3-11);

(4) The regenerated catalyst has a methanation activity and capacity for CO uptake slightly above that of the fresh (Figure 3-1 and Figure 3-3, respectively), and a TOF which is almost identical to that of the fresh catalyst.

Finding (1) indicates "dissolution" into the Raney nickel of significant amounts of carbon. Consistency with the transient-kinetic observations arises when we assume that on a 120h time scale the carbon uptake proceeds to completion for one part of the specimen, whereas the other part remains essentially free of carbon. The 120 s and 850 s transients

then reflect catalysis over, respectively, the "clean" and carbon-containing Raney nickel. The implied heterogeneity of the fresh sample could derive from bimodality in either the crystallite size, morphology or aluminum content.

4.0   ISOTOPIC TRANSIENTS STUDY ($^{12}CO/^{13}CO$ SWITCH)

ON RANEY NICKEL, 60 WT % Ni/SiO_2 AND NICKEL POWDER CATALYSTS

4.1   Background

The isotopic transient method provides an unique way to measure the fractional coverage of reaction intermediates (θ), reactivity (k) and the amount of CO_{ad} under reaction conditions. This chapter reports on an investigation of these fundamental factors (k, θ and CO_{ad}) in methanation over nickel catalysts.

4.2   Experimental

The factors k, θ and CO_{ad} were studied systematically by varying reaction conditions on Raney nickel, 60% Ni/SiO_2 and Ni powder. The total pressure was maintained at one bar. For some experiments on 60% Ni/SiO_2, the total pressure was maintained at four bar. By adding the buffering gas He, the P_{CO} and P_{H_2} were allowed to vary independently.

4.3   Results

Figure   4-1   represents   a   typical   transient   experiment $(^{12}CO + (Ar) + H_2 \xrightarrow{\quad H_2/CO = 10 \quad} {}^{13}CO + H_2)$ at   temperature 110°C.   By
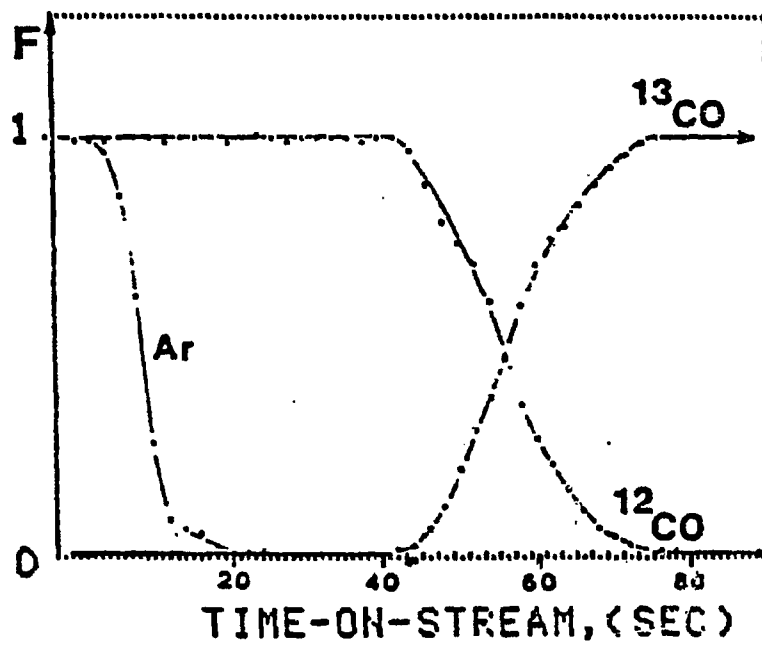
Figure 4-1 ^{12}CO (Ar) + H_2 $\longrightarrow$ ^{13}CO + H_2 at 110 $^{\circ}C$ with

H_2 / CO = 10,   60 wt % Ni/SiO_2

measuring the area between Ar and ^{12}CO curves (chromatographic effect),[25] the amount of adsorbed CO can be obtained as detailed in Chapter 2.

We assume the CO coverage at the reference condition ($110^{\circ}C$, H_2/CO = 10) to be close to unity. This assumption has been verified by independent measurements (see section 4.4.2).

The chromatographic effect allows to measure routinely the amount of adsorbed CO present at reaction conditions. Typical transient experiment results at reaction conditions are shown in Figures 4-2 and 4-3. The Θ_{CO} is defined as

$$\Theta_{CO} = \frac{CO \text{ adsorbed at reaction condition}}{CO \text{ adsorbed at reference condition}_{(110^{\circ}C)}} \qquad (4\text{-}1)$$

The Θ_{CO} vs. H_2/CO ratio at constant temperature and Θ_{CO} vs. reaction temperatures at constant H_2/CO ratio for different nickel catalysts are summarized in Figure 4-4 and 4-5. It is seen that over a large range of reaction conditions ($2 < H_2/CO < 35$; $180^{\circ}C < T < 250^{\circ}C$) Θ_{CO} is nearly constant, indicating the coverage of CO is highly independent of reaction conditions. These results agree with the results of Bell et al.[81] Literature IR studies[77,78,98] also indicate that, at reaction conditions, CO is present at near saturation coverage. The amount of adsorbed CO has also been measured in D_2, H_2 and He at the same partial pressure of CO at $110^{\circ}C$ with results showing the amount of adsorbed CO is in the order of $CO_{in\ D_2} > CO_{in\ H_2} > CO_{in\ He}$. However, the difference
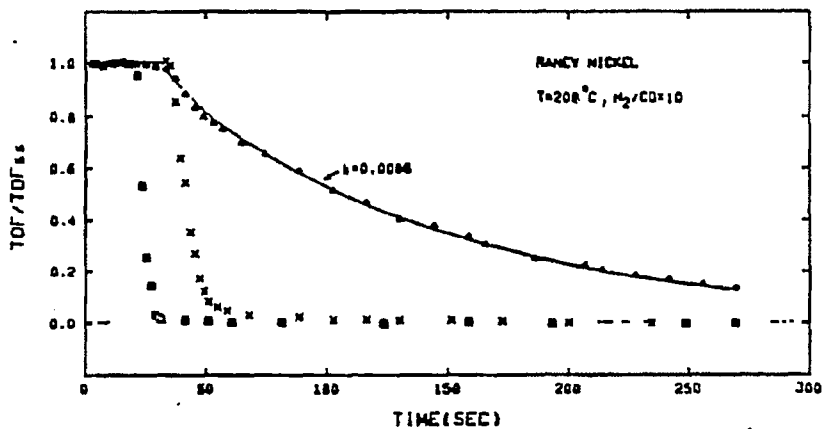
Figure 4-2 Transient response in Ar (□), ^{12}CO (x) and $^{12}CH_4$(▲) accompanying a $^{12}CO(Ar)/H_2$ to $^{13}CO/H_2$ switch. The $^{12}CH_4$ response is close to purely exponential.
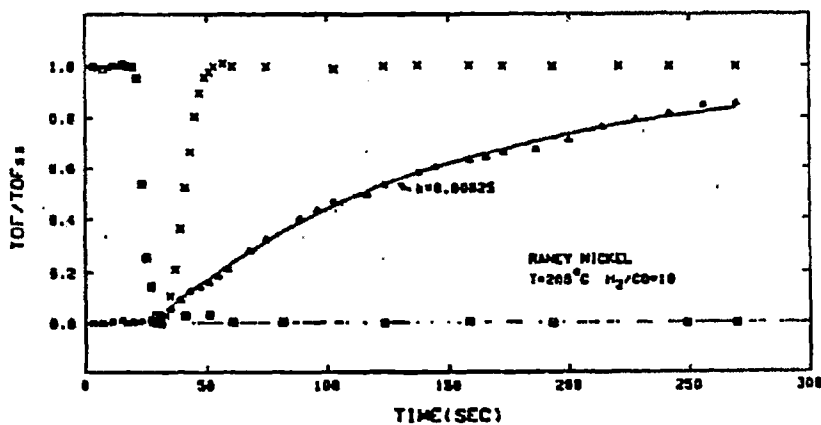
Figure 4-3 Transient response in ^{13}CO (x) and $^{13}CH_4$(▲), accompanying the same switch as that in Fig. 4-2.
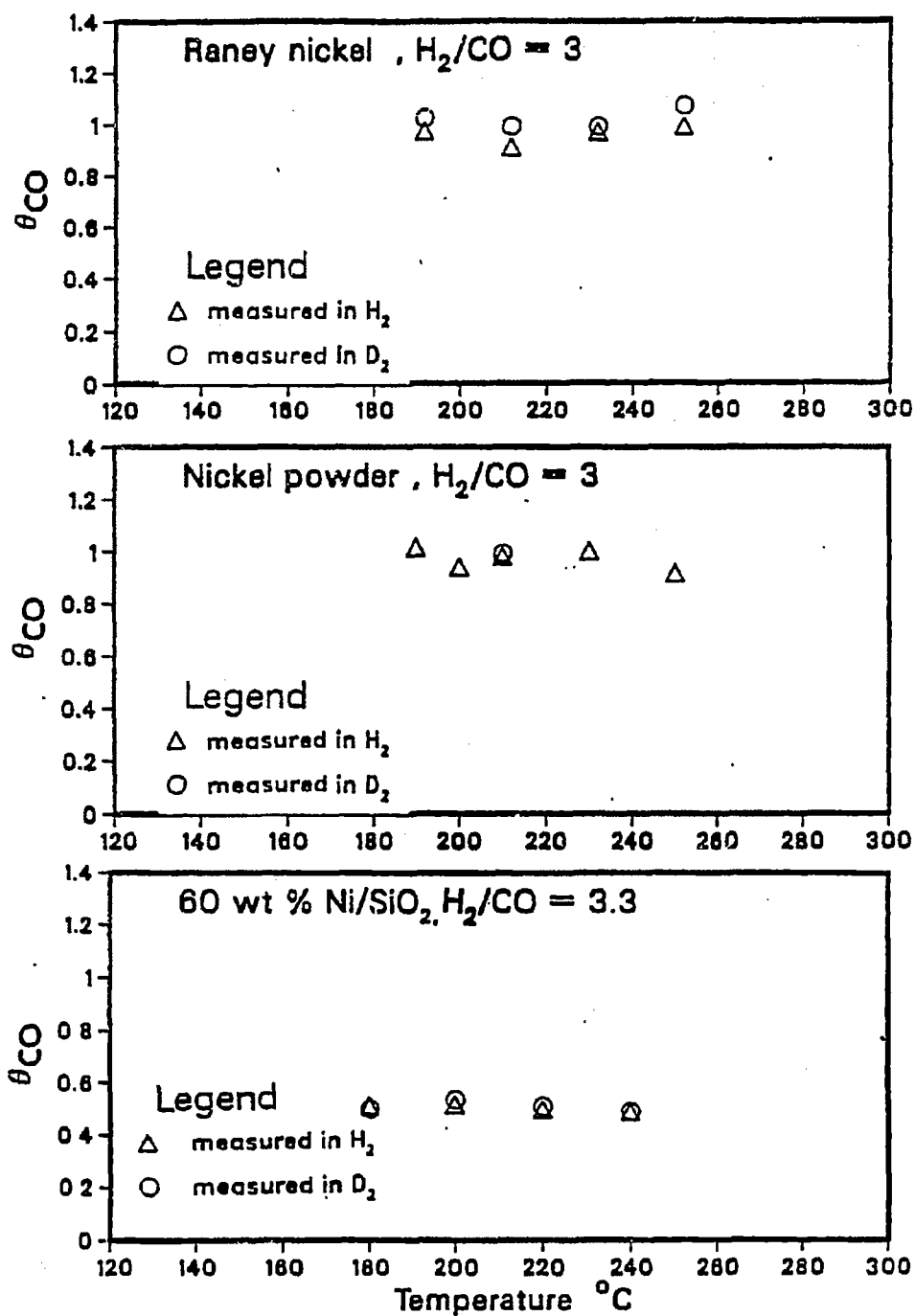
Figure 4-4   Coverage of CO versus temperature at constant
            H_2/CO with different nickel catalysts.
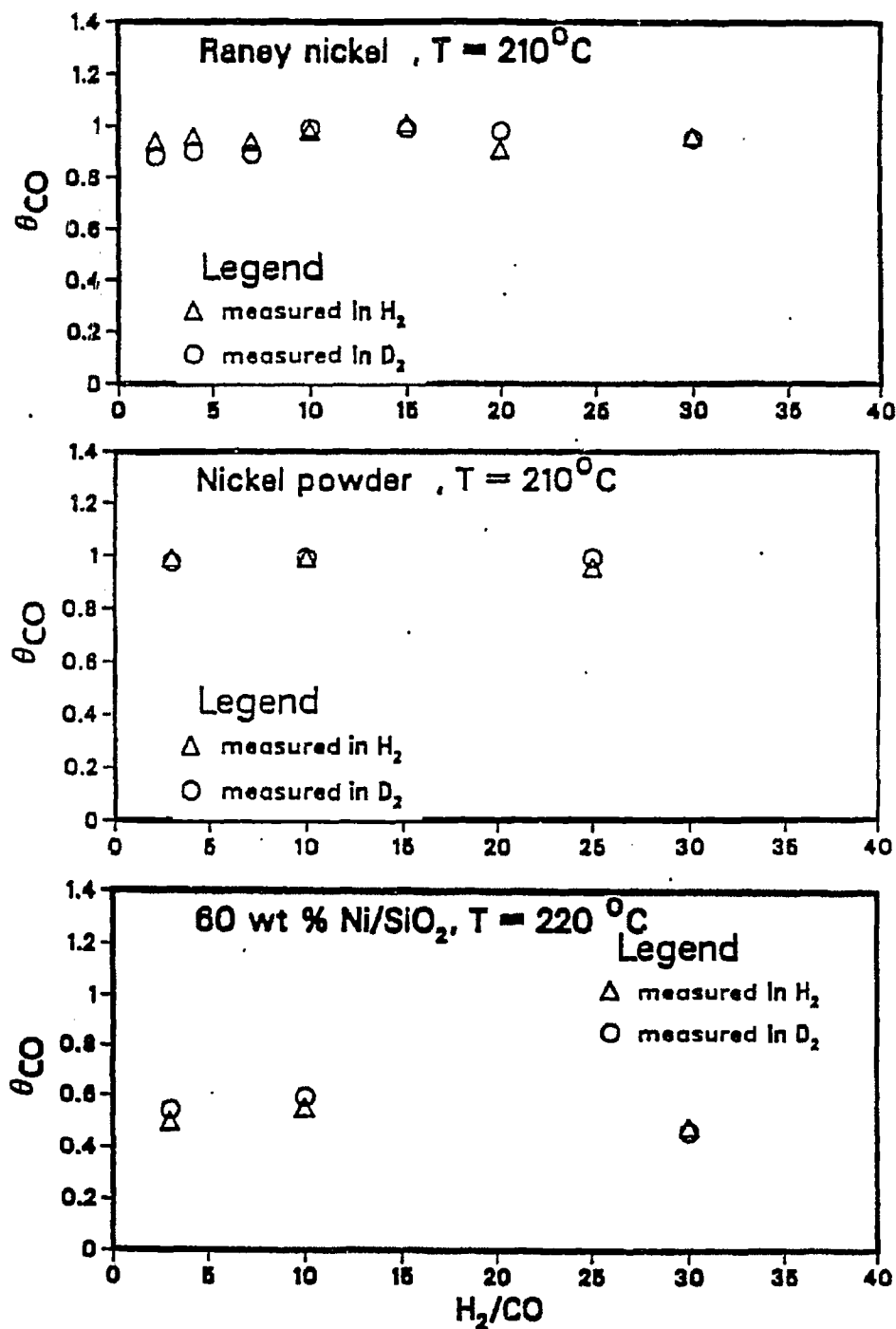
Figure 4-5 Coverage of CO versus H_2/CO at constant temperature with different nickel catalysts.

lies within a range of 2 ~ 3% of total amount of adsorbed CO being measured, which is within the range of experimental errors.

Although one paper[92] reports the amount of adsorbed CO measured in H_2 is larger than that measured in He, the result of this study, which concludes that the Θ_{co} in H_2 > Θ_{co} in He, is incorrect. Within the range of experimental errors, the amount of adsorbed CO measured in H_2 is close to that measured in He.

The coverage of CO in Raney nickel and nickel powder is close to unity. However, the coverage of CO in Ni/SiO_2 is close to half, suggesting that the nature of nickel catalysts may affect the coverage of CO. Happel et al.[10] also shows that, for methanation over Ni/SiO_2 under reaction conditions, CO_{ad} seems to occupy almost half of the total metal sites.

We also observed the amount of adsorbed CO at reaction condition either in H_2 or in D_2 is nearly equal. The supporting data is plotted in Figures 4-4 and 4-5.

The amount of carbidic intermediates, CH_x-ad, can be estimated from the transient experiment (^{12}CO + Ar + H_2 → ^{13}CO + H_2) shown in Figures 4-2 and 4-3. The detailed procedure for measuring the amount of carbidic intermediates was discussed in Chapter 2. Figures 4-6, 4-7 and 4-9 show the partial pressure dependence of the amount of carbidic intermediates, CH_x-ad on 60 wt% Ni/SiO_2. The amount of CH_x-ad varies significantly and reversibly with P_{H_2}, P_{CO} and H_2/CO ratios at constant temperature. Several features are noteworthy. The Θ_{CH_x} increases with increasing P_{H_2} and also increases with H_2/CO ratio, a trend opposite
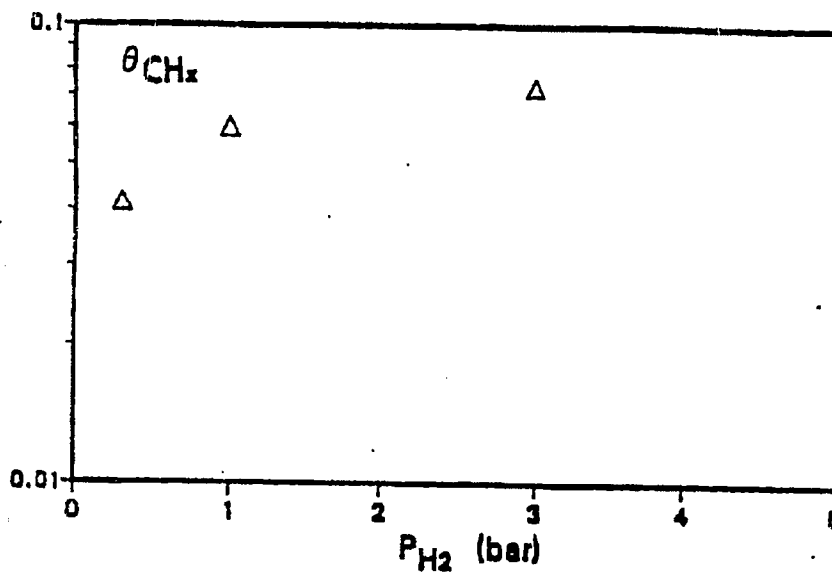
Figure 4-6 Coverage in carbidic intermediates, CH_x, versus P_{H_2}.
$P_{co} = 0.1$ bar, $T = 210°C$, catalyst : 60 wt% Ni/SiO_2
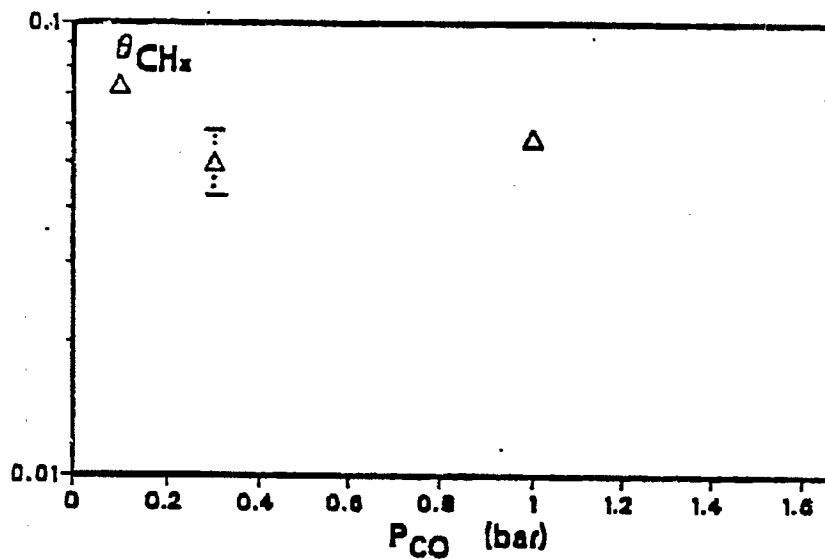
Figure 4-7 Coverage in carbidic intermediates, CH_x, versus
P_{co}. $P_{H_2} = 3$ bar, $T = 220°C$, catalyst :60 wt% Ni/SiO_2
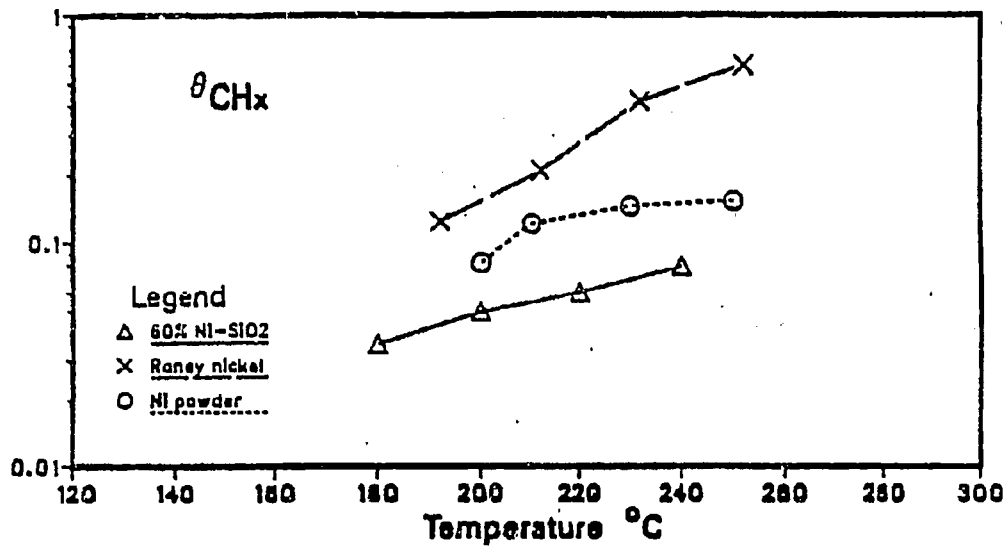
Figure 4-8 Coverage in carbidic intermediates depend on the detailed nature of the catalyst. For Raney nickel and Ni powder P_{H_2} = 0.9 bar , P_{co}= 0.09 bar. For 60 wt% Ni/SiO_2 P_{co}= 0.1 bar,

P_{H_2} = 1 bar.
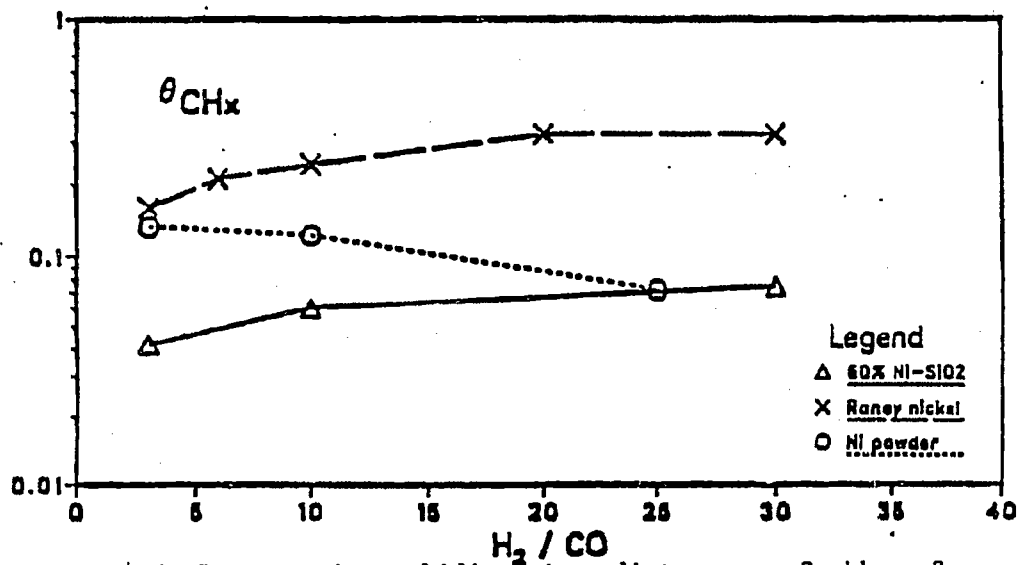
Figure 4-9 Coverage in carbidic intermediates as a fuction of H_2/CO. T = 210°C for Raney nickel and Ni powder. T = 220°C for 60 wt % Ni/SiO_2.

that reported by Goodman et al.[36] on Ni (110). The observation that Θ_{CH_x} increases with H_2/CO ratio, however, is consistent with the result reported by Zhang and Biloen.[40] The temperature dependence of the CH_x-ad is shown in Figure 4-8. The reversibility of the phenomenon displayed in Figure 4-8 can be observed: by ramping the temperature up and down, we move up and down the same $\Theta_{CH_x} = F(T)$, as long as we remain outside the $T > 250^{\circ}C$ region. The amount of carbidic intermediates which increased with temperature is in agreement with the finding of Goodman et al.[36] and Bell and Winslow.[41]. All aforementioned results pertain to 60% wt Ni/SiO_2.

The H_2/CO ratio dependence of the coverage of reaction intermediates with different Ni catalysts is presented in Figure 4-9. A large variation of Θ_{CH_x} is observed, suggesting that the coverage of the carbidic intermediates varies significantly with the nature of the catalyst. Raney nickel showed similar trend as 60 wt % Ni/SiO_2. However, an opposite trend is found with Ni powder. The trend of Θ_{CH_x} decreasing with H_2/CO ratio confirmed that. reported by Goodman et al.[36] Figure 4-8 presents the temperature dependence of the coverage of carbidic intermediates with different Ni catalysts. The results indicated that all Ni catalysts have the same trend - the Θ_{CH_x} increased with increasing temperature. This finding is in agreement with most literature data.[36,41]

However, a significant variation of Θ_{CH_x} with different Ni catalysts is also observed, leading to the conclusion that the coverage

of reaction intermediates depends on the nature of Ni catalysts. The detailed data for Θ_{CH_x} with different catalysts is listed in Table 4-1.

The reactivity of carbidic intermediates, $k = 1/\tau$, can be estimated from transient experiment ($^{12}CO + Ar + H_2 \rightarrow {}^{13}CO + H_2$) shown in Figure 4-2~3.

As shown in Figure 4-2~3, the decay of $^{12}CH_4$ and the ingrowth are, for "fresh" catalysts, close to exponential: $F = \exp [t/\tau]$. According to Equation 3-8, a single homogeneous pool/reservoir of intermediates will result in exponentially decay. This suggests that we have a single homogeneous pool/reservoir of intermediates.

Figures 4-10, 4-11 and 4-14 demonstrate the partial pressure dependence of the reactivity k ($= 1/\tau$) of carbidic intermediates. The k of carbidic intermediates varies significantly with P_{H_2}, P_{CO} and H_2/CO ratio at constant temperature on 60 wt % Ni/SiO$_2$. The k increases with increasing P_{H_2} and also increases with H_2/CO ratio. Figure 4-10 suggests that the hydrogenation reaction determines the relaxation time τ ($\tau = 1/k$).

The temperature dependence of k is shown in Figure 4-15. An increasing temperature results in an increase in the reactivity of intermediates.

Typical experimental results of the dependence of reactivity k on H_2/CO ratio and temperature are shown in Figures 4-12 and 4-13. The reactivity of reaction intermediates versus H_2/CO ratio with different Ni catalysts is demonstrated in Figure 4-14. The results indicate that all Ni catalysts follow the same trend - the k increases with increasing

Table 4-1

Coverages of Carbidic Intermediates, Reactivity and TOF Versus Reaction Conditions

Raney Nickel

T	H_2/CO	$k \times 10^{-3}$	Θ_c	$\times 10^{-4}$ TOF
192	3	9.72 ± 0.30	0.053 ± 0.002	5.19
192	6	10. ∓ 0.625	0.0877 ∓ 0.00543	8.82
192	10	10.58 ∓ 0.706	0.1254 ∓ 0.0083	13.28
212	3	12.0	0.1693	20.32
212	6	13.82 ± 1.57	0.2278 ± 0.0258	31.49
212	10	20.52	0.2166	43.223
212	20	25.84 ± 0.585	0.314 ± 0.007	81.163
212	30	32.16 ∓ 3.33	0.3302 ∓ 0.034	106.213
232	3	24.1	0.383	92.318
252	3	51	0.634	323.39

Ni Powder

T	H_2/CO	$\times 10^{-3}$ k	$\times 10^{-2}$ Θ_c	$\times 10^{-4}$ TOF
200	3	5.97 ± 0.49	8.07 ± 0.66	4.828
200	10	9.15 ∓ 1.16	8.17 ∓ 1.03	7.486
200	25	23.21	4.02 ∓ 1.01	9.349
210	3	7.03 ± 0.67	13.32 ∓ 1.28	9.368
210	10	11.85 ∓ 1.39	12.2 ∓ 1.44	14.54
210	25	25.64 ∓ 3.85	7.07 ∓ 1.06	18.15
230	3	12.85 ∓ 1.83	22.79 ∓ 3.24	29.312
230	10	31.35 ∓ 4.08	14.66 ∓ 1.91	45.97
230	25	51.1 ∓ 0.79	10.706 ∓ 0.165	54.73
250	3	30.1 ∓ 5.87	22.64 ∓ 4.4	68.36
250	10	50.04 ∓ 8.79	17.57 ∓ 3.4	87.93
250	25	83.54 ∓ 4.7	10.93 ∓ 0.624	91.39

Table 4-1 (Continued)

Coverages of Carbidic Intermediates, Reactivity and
TOF Versus Reaction Conditions

60 wt. % Ni/SiO_2

T	P_{co}	P_{H_2}	H_2/CO	$\times 10^{-3}$ k	Θ_C	$\times 10^{-4}$ TOF
180	0.1	1.	10	5.21	0.033	1.7193
200	0.1	1	10	17.3	0.049	8.477
220	0.1	1	10	22.205	0.06	13.421
240	0.1	1	10	46.4	0.0797	36.321
180	0.3	1	3.3	2.576	0.0367	0.947
200	0.3	1	3.3	5.963	0.0458	2.736
220	0.3	1	3.3	19.11	0.04808	9.19
220	0.1	0.3	3	17.138	0.0414	7.01
220	0.1	3	30	41.08	0.0733	30.13
220	0.3	3	10	43.85	0.04188	18.37
220	1	3	3	15.68	0.05637	8.842
240	0.3	1	3.3	53.106	0.0466	24.766
240	0.1	0.3	3	24.34	0.0804	19.58
240	0.3	3	10	127.6	0.0403	51.49
240	1	3	3	48.12	0.0524	25.26
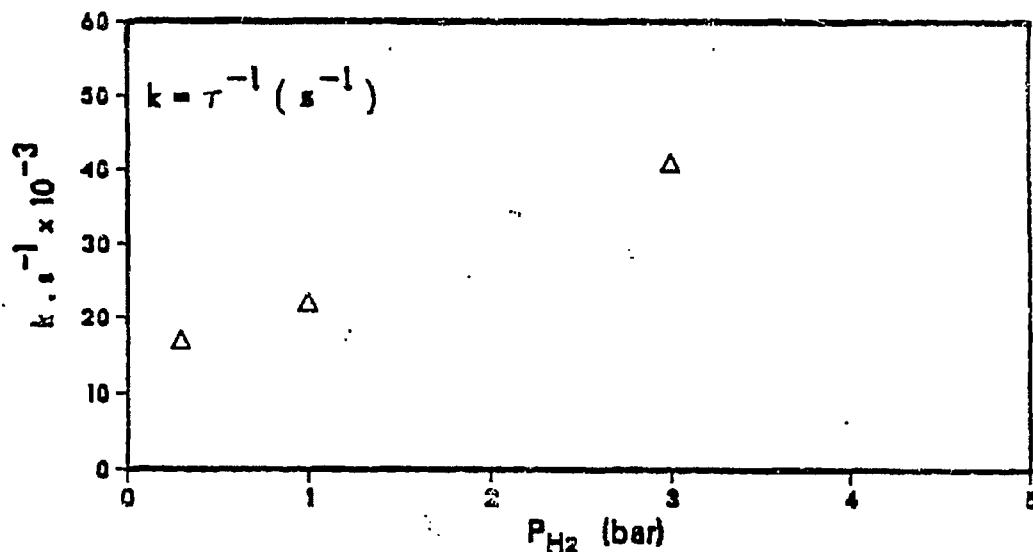
Figure 4-10 The reactivity of carbidic intermediates increases
with increasing P_{H_2} . P_{co}= 0.1 bar, T = 220 ^{o}C, catalyst: 50 wt %
Ni/SiO_2.
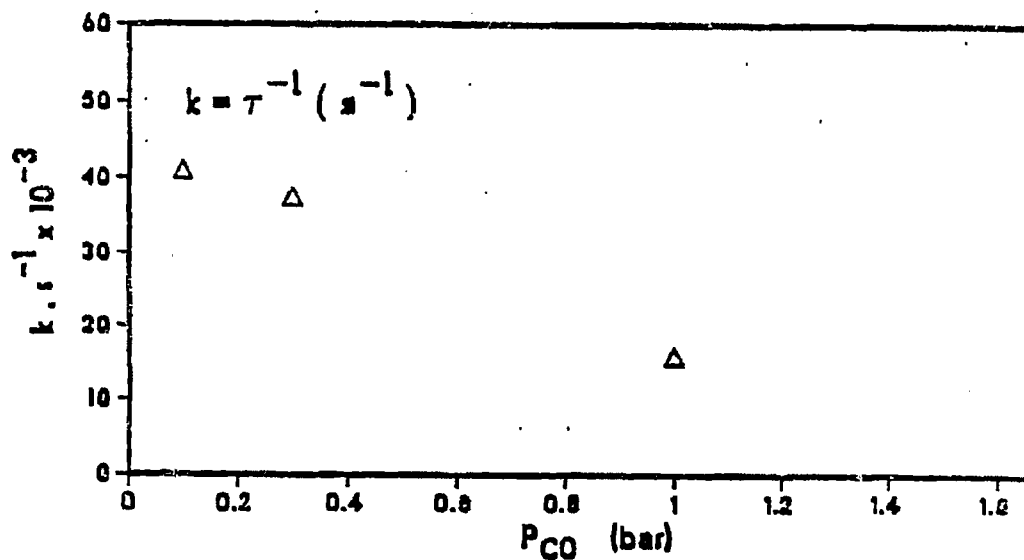
Figure 4-11 The reactivity of carbidic intermediates decreases
with increasing P_{co} . P_{H_2}= 3 bar, T = 220 ^{o}C, catalyst: 60 wt %
Ni/SiO_2.
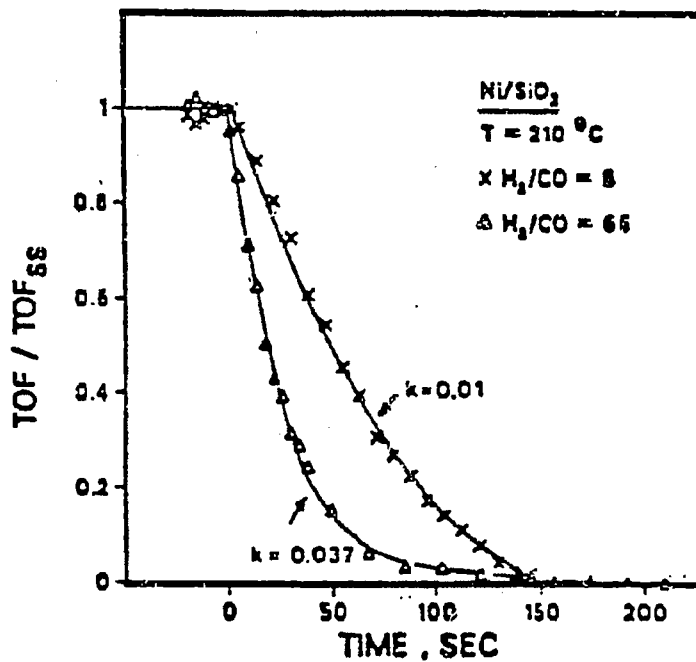
Figure 4-12 Reactivity of carbidic intermediates versus H_2/CO ratio.
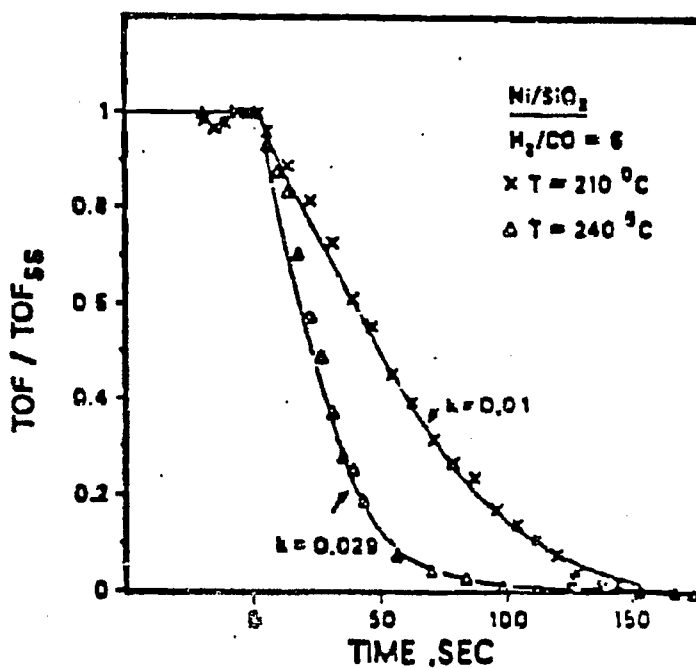
Figure 4-13 Reactivity of carbidic intermediates versus temperature.
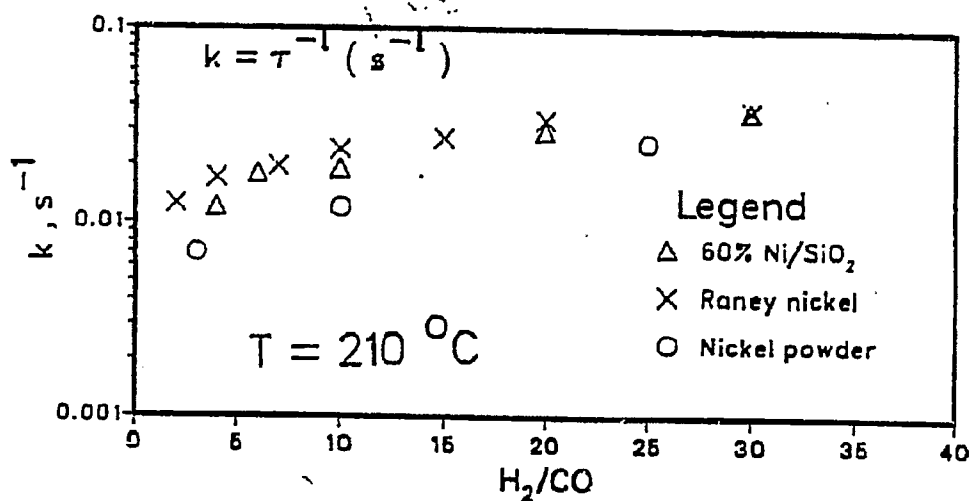
Figure 4-14 Reactivities of carbidic intermediates versus H_2/CO ratio at constant temperature with different nickel catalysts.
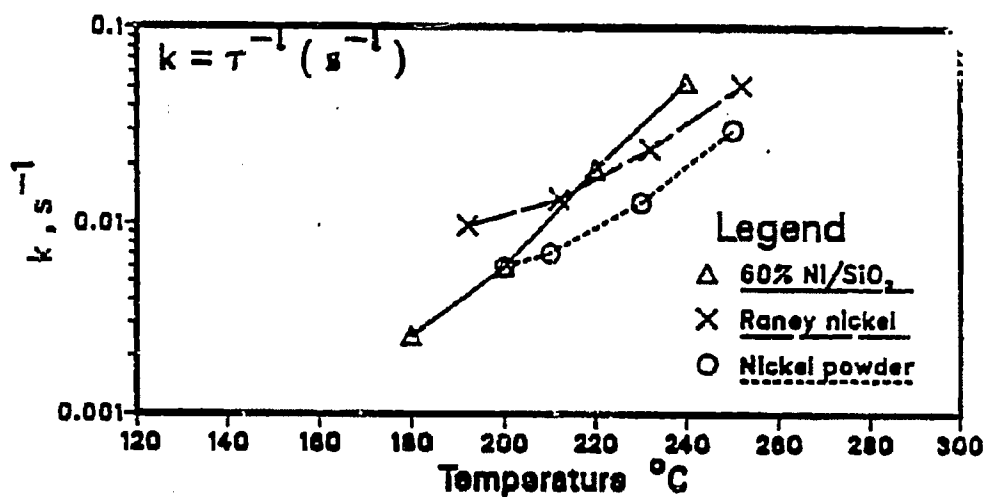
Figure 4-15 Reactivities of carbidic intermediates depend on the detailed nature of the catalyst. For Raney nickel and Ni powder P_{H_2} = 0.75 bar, P_{co}= 0.25 bar. For 60 % Ni/SiO$_2$

P_{co}= 0.3 bar, P_{H_2} = 1 bar.

H_2/CO ratio. This finding suggests a hydrogenation reaction determines the relaxation time τ (= $1/k$). A variation of k with different catalysts is observed (Figure 4-15). It indicated that the reactivity of carbidic intermediates varies with the nature of the nickel catalysts.

Figure 4-15 presents the temperature dependence of the reactivity of carbidic intermediates with different Ni catalysts. The results indicate that all Ni catalysts follow the same trend - the k increases with the temperature. However, a significant variation of k is observed with different Ni catalysts. This observation suggests that the reactivity of the carbidic intermediates varies with the nature of the nickel catalysts. The detailed data for k with different catalysts is presented in Table 4-1.

Figure 4-16 displays the Arrhenius plot for methane formation with different Ni catalysts. The activation energy for methanation reaction does not change as a function of the reaction temperature. The activation energies for Raney nickel, Ni powder and Ni/SiO_2 are 31, 28 and 25 kcal/gmole, respectively. This apparent activation energy is in close agreement with literature data.[3,21,58,91] From the variation of TOF with different Ni catalysts, an order of Raney-Ni > Ni powder > Ni/SiO_2 is observed. The relative order for TOF is comparable with literature results[43,58]. Since the variation of TOF is less than 10 times, according to Boudart's definition the methanation should be classified as a structure insensitive reaction. However, in this study the nature of Ni catalysts do have an observable effect on the TOF in

91
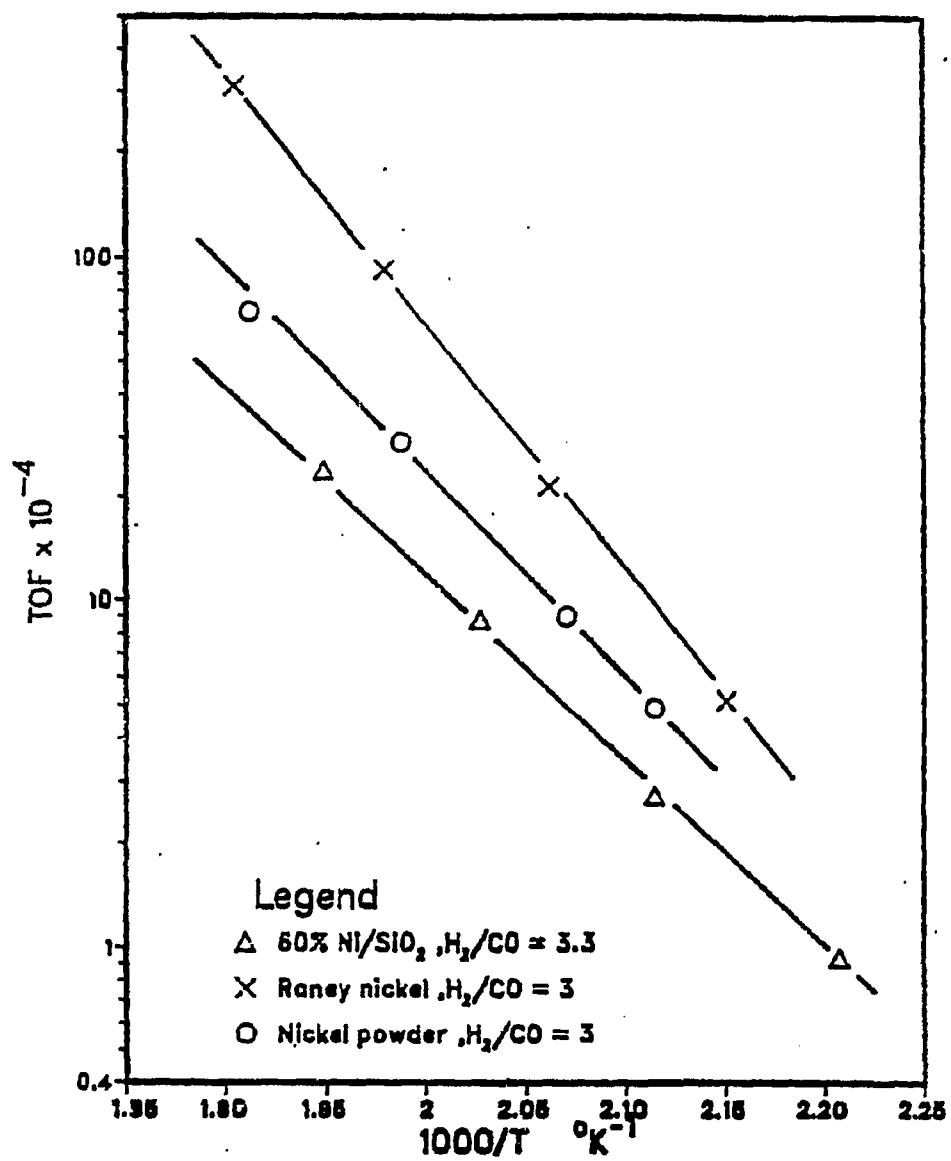
Figure 4-16   Arrhenius plots for different nickel catalysts.

methanation. The steady-state catalytic behavior of nickel catalysts is summarized in Table 4-2 together with literature data from other investigators.

Here all Arrhenius and partial pressure dependency data have been interpreted to give the parameters in a power rate law of the form

$$N_{CH_4} = k \, P_{H_2}^{x} \, P_{CO}^{y} \qquad (4-2)$$

where N_{CH_4} is the turnover number for CH_4 formation expressed as molecules of CH_4 formed per second per surface-exposed atom. $k = A \exp (-E/RT)$, E is the activation energy, and P_{H_2} and P_{CO} are the partial pressure of H_2 and CO, respectively. Assuming the activation energy E and the orders of the reaction x and y are independent of the H_2 and CO partial pressures and temperatures, the E, x and y can be determined by the variation of temperature, P_{CO} and P_{H_2}, respectively. In view of the large variations in experimental conditions, our data agrees with most literature data.

When the surface of Raney nickel is deliberately covered with "hard" carbon, via short exposures to pure CO at 300°C, the TOF and the amount of CO adsorbed decrease proportionally, as shown in Figure 4-17. The conclusion emerges from deliberate carbon deposition experiments that CO does not adsorb on top of "hard" surface carbon.

Table 4-2

Steady State Kinetic Behavior

$$N_{CH_4} = kP_{H_2}^x \, P_{co}^y$$

Catalyst	X	Y	E (kcal/g mole)	
Raney nickel	1.05 ± 0.06	-0.77 ± 0.04	31	(in this study)
60 wt % Ni/SiO$_2$	0.66 ± 0.03	-0.54 ± 0.07	25	
Ni powder	0.92 ± 0.05	-0.43 ± 0.04	28	
Raney Ni	-	-	31.9	(91)
	-	-	31.02	(21)
10% Ni/SiO$_2$	-	-	25	(3)
20% Ni/SiO$_2$	0.91~1.03	-0.39~ -0.47	20.9	(7)
All nickel catalysts	0.6~0.8	-0.2~ -0.5	25-33	(58)
Ni powder	1.04 ± 0.4	-0.4 ± 0.05	-	(67)
Ni powder	-	-	27.95	(91)
Ni metal	-	-	28.9	(21)
Ni metal	-	-	32	
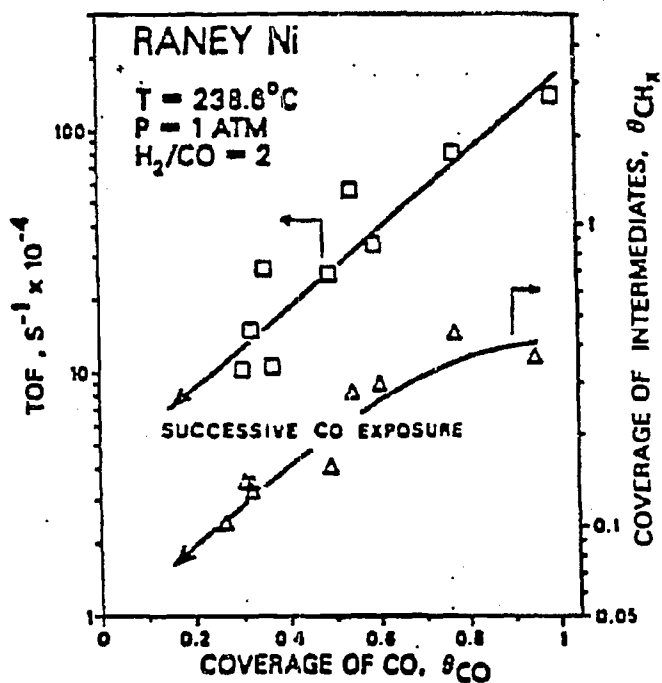
Figure 4-17 Successive carbon depositions (short exposures to CO at 300 °C) on Raney nickel.
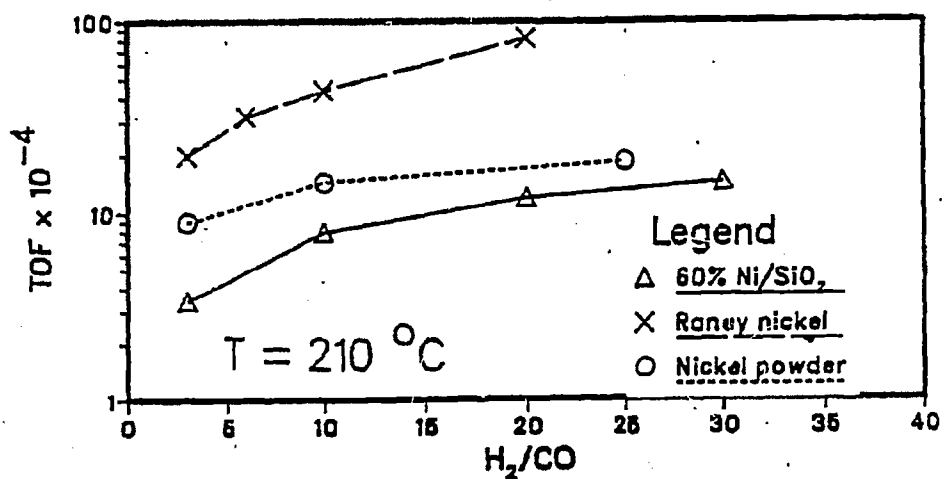
Figure 4-18 TOF versus H_2/CO ratio with different nickel catalysts.

4.4 DISCUSSION

4.4.1 Low Value of Θ_{CH_x}

In their study Biloen et al.[25] suggest that the synthesis rate for methane was limited by a low value of the intermediates. The majority of the available catalyst surface probably had been blocked by unreactive carbon (site blocking effect) which could have led to the low Θ values. From this study the observation emerges that, for methanation over nickel, the surface blocking by unreactive carbon is not controlling the coverage in reactive intermediates. The reasons are discussed below.

From Figure 4-17 the deliberate carbon deposition experiments, it was found that CO does not adsorb on top of "hard" surface carbon. It was further observed that within a significant range of experimental conditions (i.e., $T \leq 250$, $H_2/CO \geq 2$) the in-situ measured CO_{ad} values are essentially time independent and close to the value measured prior to reaction at $110^{\circ}C$, i.e., on the fresh nickel surface. These two observations, when combined, suggest a largely unblocked surface. The observation that the low Θ_c value is not due to site blocking by unreactive carbon is in agreement with the results reported by Happel et al.[10] and Bell et al.[38]. The small coverages in unreactive carbon

and oxygen appear to inhibit the CO dissociation, thereby limiting the steady-state production of carbidic reaction intermediates (see 4.4.4).

4.4.2 Comparison of Transient Methods With Other Independent Measurements in CO_{ad}

The formation of nickel carbonyl may affect the CO_{ad} transient measurements. If this is the case, then our result (from $^{12}CO/^{13}CO$ switch at 110°C) will show higher value of CO_{ad} than that from different measurement methods.

In Table 4-3, CO_{ad} transient ($^{12}CO/^{13}CO$ switch at 110°C) measurements in this study is compared to those of the other investigators with different measurement methods. Despite the totally different methods, the agreement in the results is excellent, confirming the validity of the transient CO_{ad} measurement in measuring the surface exposed Ni atoms. The comparison further indicates that the CO_{ad} transient measurements did not suffer from the formation of nickel carbonyl.

4.4.3 CO_{ad} and CO Dissociation

How can mechanistic information be inferred from transient experiments?

Table 4-3

Comparison of CO_{ad} Measurements

	ml/g	ml/g	BET Area $\frac{m^2}{g}$
Raney nickel	6^a	6.6^c	-
60 wt % Ni/SiO$_2$	15.2^a	14^d	-
Ni powder	0.5^a	-	
	(0.89^b $\frac{m^2}{g}$)		1.8^e

---

a   Transient measurement $^{12}CO/^{13}CO$ switch at 110°C $H_2/CO \geq 10$.

b   Surface area is calculated by assuming CO/M = 1/1.

c   Dr. D. G. Blackmond's CO chemisorption measurements are gratefully acknowledged.

d   CO chemisorption data at room temperature in reference[10].

e   One point BET surface area measurement was conducted by Exxon research laboratory.

Results from many studies indicate that the adsorbed CO is in equilibrium with gas phase CO under reaction condition.[10,82] This phenomenon can also be observed by transient studies. Figures 4-2 and 4-3 demonstrate this phenomenon.

As shown in Figures 4-2 and 4-3, the adsorbed ^{12}CO is quickly replaced by ^{13}CO. This suggests that the gas phase CO and adsorbed CO is in equilibrium, i.e. $(CO_{(g)} \leftrightarrow CO_*)$. The equilibrium for $CO_{(g)} \leftrightarrow CO*$ under reaction condition is established.

Figure 4-5 shows the amount of adsorbed CO to be highly independent of H_2/CO ratio under reaction condition. However, Figure 4-18 displays the TOF of CH_4 dependence on H_2/CO ratios. The total methane production increases with the H_2/CO ratio. These observations suggest the reaction pathways charted in Figure 4-19.

Most adsorbed ^{12}CO is desorbed as $^{12}CO_{(g)}$ in a reversible fashion, i.e. $(r_0 \simeq r_{-0})$. The adsorbed rate r_0 and desorbed rate r_{-0} are much larger than the dissociation rate r_1, i.e., $(r_0 \simeq r_{-0} \gg r_1)$. This results in a Θ_{CO} highly independent of the H_2/CO ratio. Results graphed in Figures 4-2 and 4-3 also indicate that, after the removal of all the $^{12}CO_{ad}$, the $^{12}CH_4$ production still continues for a sufficiently long time. This information suggests that the $^{12}C_{ad}$ transfers predominantly to the product $^{12}CH_4$ rather than reactant ^{12}CO, i.e. $(r_1 \gg r_{-1})$. The dissociation of CO_{ad} is essentially a unidirectional step. With the above observations considered together, the following hypothesis is formulated. The formation of methane is strongly associated with C_{ad} in
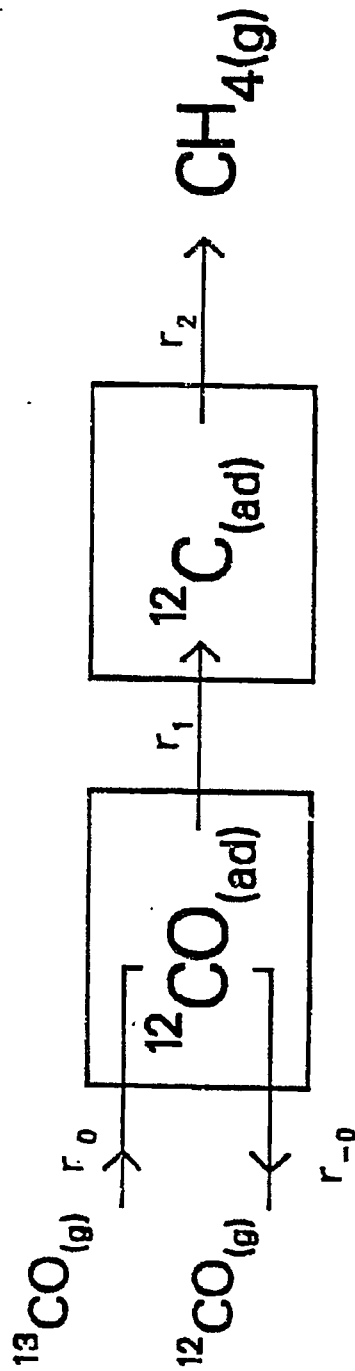
Figure 4-19 Simplified reaction pathway scheme for methanation. For the case $r_0 \approx r_{-0} \gg r_1 \gg r_{-1}$, the $^{12}CO_{ad}$ transfers predominantly backward, and $^{12}C_{ad}$ predominantly forward

either the formation of C_{ad} (r_1) or the further reaction of C_{ad} (r_2). The first two steps of methanation are

$$CO_{(g)} \xrightarrow{\quad o \quad} CO_{ad} \tag{4-3}$$

$$CO_{ad} \xrightarrow{\quad 1 \quad} C_* + O_* \tag{4-4}$$

The $r_0 \approx r_{-0} \gg r_1 \gg r_{-1}$ explains both, the Θ_{co} not being a function of H_2/CO ratio, and the methane production being a function of H_2/CO ratio. The H_2/CO ratio effect on C_{ad} can be seen in Figures 4-9 and 4-14.

Many questions arise regarding the CO dissociation step. Does the CO dissociation involve the CH_nO species? Is the CO dissociation very fast or very slow?

Vannice[21,58] proposed a reaction scheme which involved the dissociation of CH_nO species being a slow step based on steady-state kinetics information. However, Biloen and Sachtler[8] indicated that, based on the same steady-state kinetics data, a mechanism not involving CH_nO species can also be established. It is clear that different mechanisms can be formulated when based on the LHHW approach and on steady-state kinetics.

Mori et al.[7] also proposed a mechanism, involving the dissociation of CH_nO as a slow step. However, the methodolgy of Mori's study was PSRA (pulse studies surface reaction analysis) i.e., suddenly injecting a pulse of CO in constant flowing H_2 at reaction conditions.

The involvement of CH_nO species is the case in which the dominated surface species are H* with small amount of adsorbed CO (no desorbed CO is observed by Mori). Under normal methanation conditions the dominated surface species are CO_{ad} ($CO_g \leftrightarrow CO*$), C*, and some H*. It is possible that different surface conditions result in different mechanisms. If the CH_nO species does exist under reaction conditions, what will the transient result look like?

Recently, Biloen and coworkers[31] reported a comparison of nickel and platinum-catalyzed methanation, utilizing transient-kinetic methods at comparable reaction conditions. The result is shown in Figure 4-20. As seen in Figure 4-20a and Figure 4-20b, it indicates that the lifetime of platinum-bond intermediates is two orders lower than that of nickel-bonded intermediates. Two orders difference in magnitude of τ ($\tau_{Ni} \gg \tau_{pt}$) and Θ ($\Theta_{Ni} \gg \Theta_{pt}$) at comparable TOF of methane is observed. Different reaction pathways are indicated, i.e.,

$$\xrightleftharpoons{} CH_xO \xrightarrow[-H_2O]{r} CH_x \xrightleftharpoons{} (Ni) \qquad (4\text{-}5)$$

$$\xrightleftharpoons{} CH_yO \xrightarrow[-H_2O]{r} CH_y \xrightleftharpoons{} (Pt) \qquad (4\text{-}6)$$
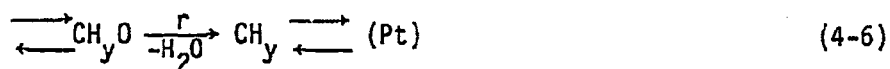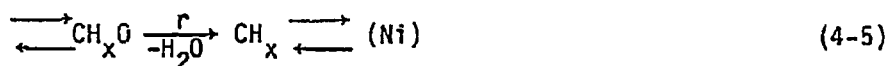
with $x < y$. x equals to zero.

Comparing Figure 4-2 with Figure 4-20, similar transient reponses in ^{12}CO and $^{12}CH_4$ are observed. There is a significant difference between these two transient responses. This difference suggests that the methanation over Raney nickel may not involve a CH_nO species.

102
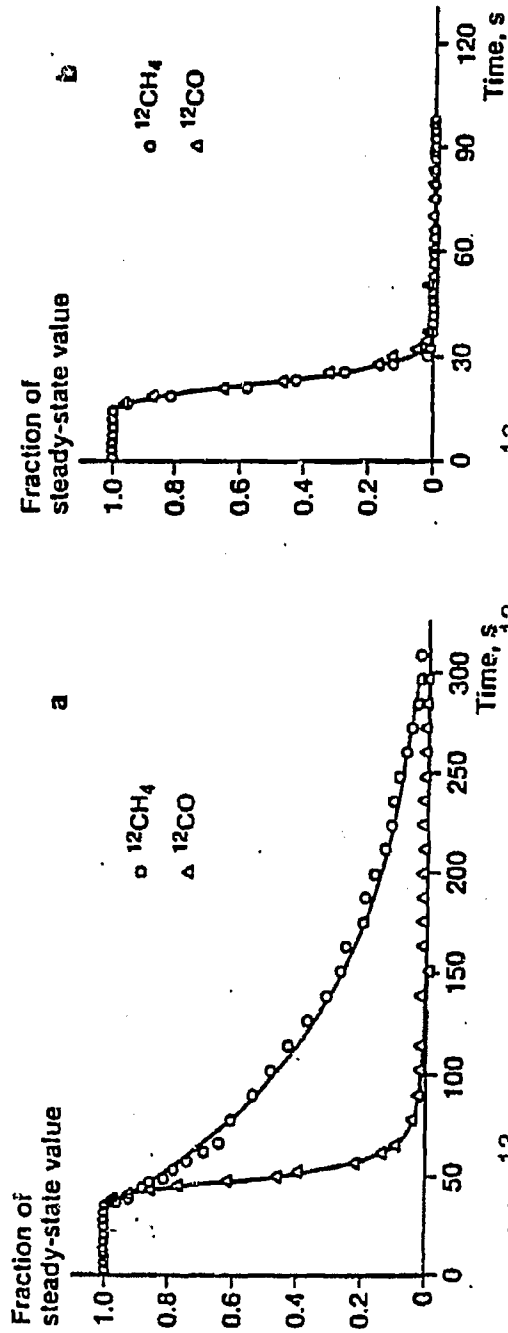
Figure 4-20 (a) $^{12}CH_4$ response when switching from $^{12}CO/H_2$ to $^{13}CO/H_2$ over nickel. The production of $^{12}CH_4$ in $^{13}CO/H_2$ atmosphere continues for approximately 100 s. (b) $^{12}CH_4$ response when switching from $^{12}CO/H_2$ to $^{13}CO/H_2$ over platinum. In $^{13}CO/H_2$ atmosphere the production of $^{12}CH_4$ ceases immediately.

Similar transient reponses in ^{12}CO and $^{12}CH_4$ (same as in Figure 4-20a) are also observed in nickel powder. The same conclusion (not involving a CH_nO species) is also valid for nickel powder.

Experimental evidence in support of the partially hydrogenated CH_nO surface species was inferred mostly from coadsorption of H_2 and CO where the mutually enhanced adsorption implies surface compound formation.[75,134] A large amount of H_2 was observed to coexist with the CO under reaction condition (see Figures 6-15, 6-16, 6-17). This does not necessarily imply the formation of CH_nO species. The H may associate with $C\beta$ in the form of $C_\beta H_y$ or may associate with metal sites.[83,38] Dalla Bella and Shelef [2] claim that the dissociation of CO is a slow step based on the absence of H/D isotope effect. However, Wilson [69] pointed out the absence of H/D isotope effect is insufficient to suggest the dissociation of CO as a slow step. The H/D isotope effect may come from the combination of kinetic and thermodynamic isotope effect (see Chapter 5).

It has been suggested by TPR (Temperature Programmed Reaction) studies[91,119] that uissociation of CO is the rate-determining step. Again, the reaction conditions under TPR study may not represent the actual methanation condition. The condition of TPR is similar to PSRA. It is not surprising that extremely different surface conditions result in different mechanisms.

The work by Biloen et al.[25,26] (isotopic transient methods) and Bell et al.[82] (isotopic transient methods) has shown that the dissociation of adsorbed CO appears to be irreversible and very fast.

Goodman and Yates [93] also indicated that the irreversibility of the CO dissociation and the absolute rates of CO dissociation is sufficiently rapid to account for all the methane production over Ni. Up to this point, the following hypothesis can be formulated.

The CO in the gas phase is virtually in equilibrium with adsorbed CO. The H-unassisted dissociation of CO is essentially irreversible.

4.4.4 Mechanistic Information Inferred from k and Θ

A simplified reaction path way is illustrated as follows:

$$CO_{ad} \xrightarrow[-H_2O]{k_1} C_{ad} \xrightarrow[+H]{k_2} CH_4(g) \qquad\qquad \text{Scheme (B)}$$

where k_2 and $\Theta_{C_{ad}}$ are measured through transient experiments.

Figure 4-10 represents the P_{H_2} effect on k_2. As k_2 increases with P_{H_2}, probably one of the hydrogenation steps of C_{ad} is rate limiting. Figure 4-14 displays the H_2/CO ratio effect on k_2 with different nickel catalysts. It seems that all nickel catalysts in this study follow the same trend. k_2 increases with H_2/CO ratio, which suggests the same hypothesis that one of the hydrogenation steps in surface carbon is rate limiting. However, for two (Raney nickel, Ni/SiO_2) out of three nickel catalysts, $\Theta_{C_{ad}}$ also increases with P_{H_2} (Figures 4-9).

From the results shown in Figure 4-5, it can be seen that Θ_{CO} remains virtually constant. Since $k_1\Theta_{CO} = k_2\Theta_{C_{ad}}$ (Figure 4-19), it is concluded that k_1 increases with P_{H_2}. This is seemingly inconsistent

with step 1, (Scheme 8) which is a hydrogen-unassisted dissociation step. The possible explanations are discussed below. It is possible that with variation in P_{H_2}, varying low levels of $C_{irreactive}$ or O_{ad} occur.

The amount of total carbon and total oxygen containing species can be measured by conducting the following transients ($^{12}CO + H_2 \rightarrow H_2$). The upper limit of carbon on the surface can be estimated by integrating the area under the CH_4 curves. The upper limit of oxygen-containing species on the surface can also be estimated by integrating the area under the H_2O curve. The typical results are shown in Figures 4-21,4-22, and 4-23 for Raney nickel, Ni/SiO$_2$ and Ni powder, respectively. The detailed results are summarized in Table 4-4. As listed·in·Table 4-4, total carbon and total oxygen-containing species on the catalyst is large (except for oxygen-containing species in Ni powder). The total carbon includes C_{dis} (carbon from CO dissociation after switching off CO), C_{irr} (irrective carbon), and C_{ad} (reactive carbon). The total oxygen included O_{dis} (oxygen from CO dissociation after switching off CO) and O_{ad} (oxygen associate with Ni metal and associate with support). The different H_2O transient response in nickel powder (Figure 4-23) observed suggests that part of the oxygen species in Raney nickel and Ni/SiO$_2$ is associated with support (SiO$_2$, and Al$_2$O$_3$ in Raney nickel).

Winslow and Bell recently demonstrated that low levels of "C_β" build up in the first three hundred seconds of exposure of the clean (ruthenium) surface to CO/H$_2$.[41] In general, the transient
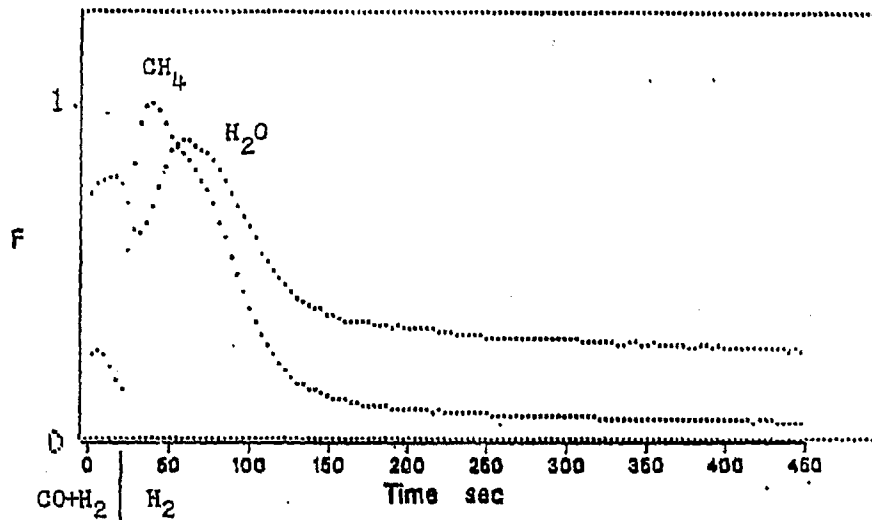
Figure 4-21 Methane and water production in pure H_2 on
Raney nickel $T = 192\ ^{o}C$, $H_2/CO = 30$
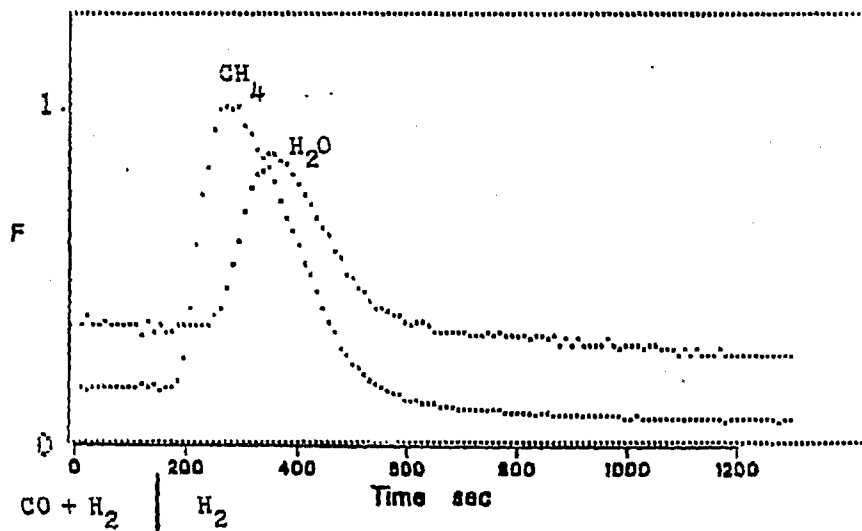
Figure 4-22 Methane and water production in pure H_2 on
60 wt % Ni/SiO_2 , $T = 180\ ^{o}C$, $H_2/CO = 3.3$, $P_{co} = 0.3$ bar.
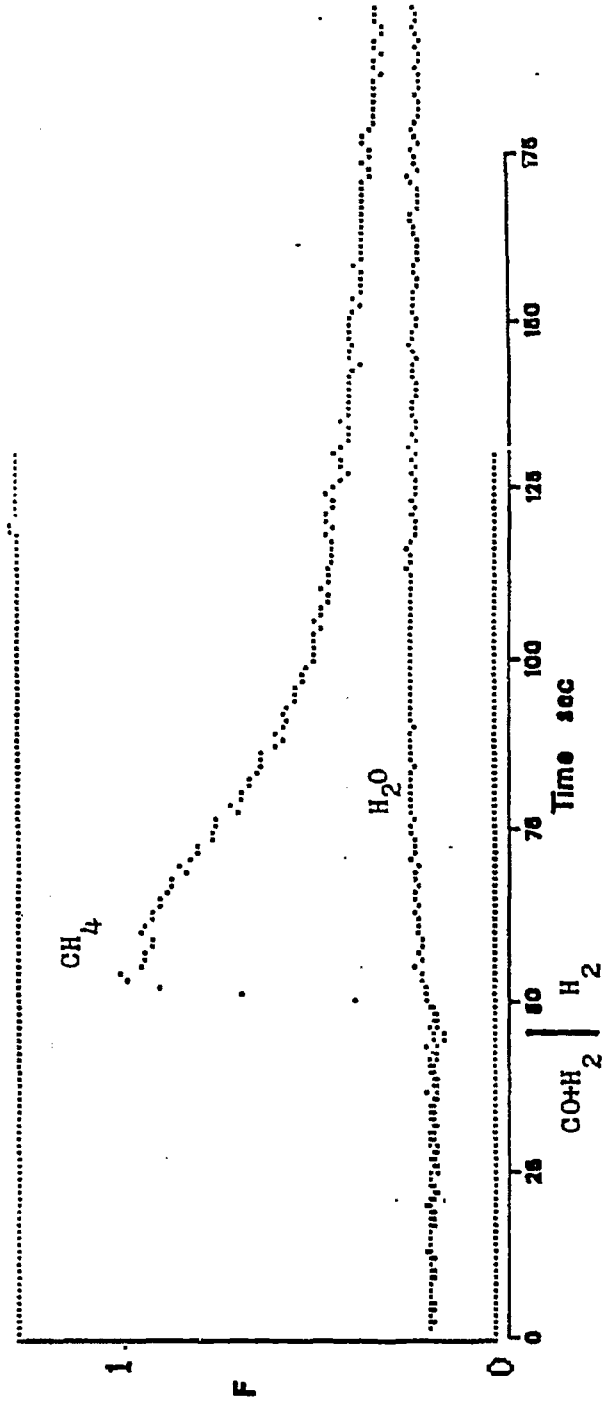
Figure 4-23 Methane production in pure H_2 on nickel powder, T = 220 ^{o}C, $H_2/CO=3.3$

Table 4-4

Result from $^{12}CO + H_2 \rightarrow H_2$ with Different Nickel Catalysts

Catalyst	T(^{O}C)	P_{co}	P_{H_2}	H_2/CO	ΘC_{tot} [a]	ΘC_{ad} [b]	ΘO_{tot} [c]
Raney nickel	192	-	-	6	1.56	0.09	0.09
(P_{tot} = 1 bar)	192	-	-	30	1.09	0.24	0.23
	212	-	-	6	1.53	0.22	0.13
	252	-	-	6	2.33	-	-
Ni powder	200	-	-	3	0.183	0.081	-
(P_{tot} = 1 bar)	200	-	-	25	0.069	0.038	-
	210	-	-	25	0.092	0.091	-
	230	-	-	25	0.141	0.107	-
	250	-	-	25	0.285	0.109	-
60% Ni/SiO$_2$	180	0.3	1	3.3	0.463	0.0367	0.036
(P_{tot} = 4 bar)	200	0.3	1	3.3	0.239	0.0458	0.0953
	220	0.3	1	3.3	0.402	0.0467	-

ΘC_{tot} [a] = total carbon on the surface measured by $^{12}CO + H_2 \rightarrow H_2$ (convert to equivalent CO monolayer taken CO uptake at 110°C as one monolayer)

ΘC_{ad} [b] = fractional coverage of CH_x measured by $^{12}CO + H_2 \rightarrow$ $^{13}CO + H_2$

ΘO_{tot} [c] = total oxygen on the surface measured by $^{12}CO + H_2 \rightarrow H_2$ (convert to equivalent CO monolayer)